

STEREO observations of stars and the search for exoplanets

K.T. Wraight¹, Glenn J. White^{1,3}, D. Bewsher² and A.J. Norton¹

¹*Department of Physics and Astronomy, The Open University, Milton Keynes, MK7 6AA, UK*

²*Jeremiah Horrocks Institute, University of Central Lancashire, Preston, Lancashire, PR1 2HE, UK*

³*Space Science and Technology Department, STFC Rutherford Appleton Laboratory, Chilton, Didcot, Oxfordshire, OX11 0QX, UK*

17 January 2021

arXiv:1103.0911v1 [astro-ph.SR] 4 Mar 2011

The feasibility of using data from the NASA *STEREO* mission for variable star and asteroseismology studies has been examined. A data analysis pipeline has been developed that is able to apply selected algorithms to the entire database of nearly a million stars to search for signs of variability. An analysis limited to stars of magnitude 10.5 has been carried out, which has resulted in the extraction of 263 eclipsing binaries (EBs), of which **122** are not recorded as such in the SIMBAD online database. The characteristics of the *STEREO* observations are shown to be extremely well-suited to variable star studies with the ability to provide continuous phase coverage for extended periods as well as repeated visits that allow both short and long term variability to be observed. This will greatly inform studies of particular stars, such as the pre-cataclysmic variable V471 Tau, as well as entire classes of stars, including many forms of rotational variability. **The high-precision photometry has also revealed a potentially substellar companion to a bright ($R = 7.5$ mag) nearby star (HD 213597), detected with 5σ significance. This would provide a significant contribution to exoplanet research if follow-up observations ascertain the mass to be within the planetary domain. Some particularly unusual EBs from the recovered sample are discussed, including a possible reclassification of a well-known star as an EB rather than a rotational variable (HR 7355) and several particularly eccentric systems, including very long-period EBs.**

Keywords: methods: data analysis – binaries: eclipsing – space vehicles: *STEREO* – stars: individual: HD 213597 – stars: individual: NSV 7359 – stars: individual: V 471 Tau

1 INTRODUCTION

The *STEREO* mission consists of two satellites in heliocentric orbit, each observing the solar environment from the Sun's atmosphere out to the Earth's orbit and together producing 3D images of this region (Kaiser et al. 2008). The HI-1 imager on the Ahead spacecraft (HI-1A) has been used to conduct a survey for variability of stars down to magnitude 12 in its field of view (within about 20 degrees of the Ecliptic Plane, see Figure 1). The lightcurves produced have been analysed to look for exoplanet transits and eclipsing binaries. The value of eclipsing variables in studies of stellar properties and evolution is well-known (de Mink et al. 2010) and the trends from this sample, as well as some particular stars of interest, will prove informative. **The detection of many new eclipsing binaries around comparatively bright stars, previously undetected in many cases due to shallow eclipses, allows for the detailed follow-up required to improve upon existing models of stellar evolution and behaviour.** Also of note is a comparison of the effectiveness of different algorithms in extracting the signatures of eclipsing binaries of different types.

The rest of this paper is divided into sections giving an overview of the *STEREO*/HI-1A characteristics, describing the data analysis pipeline, the results obtained, prospects for further study, the conclusions that can be drawn and the table showing all 263 EBs is given at the end.

Further research is being undertaken to identify and characterise other kinds of variability, which will be the subject of future papers. Some HI-1B data has been extracted (for a region between 50 and 60 degrees right ascension and 10 and 20 degrees declination, which includes a variety of interesting objects, e.g. V 471 Tau - see Section 4) but this has not yet been analysed on a large scale. The HI-1B imager is on the side of the spacecraft facing the direction of travel and the lightcurves show artefacts resulting from micrometeorite impacts, complicating the task of signal extraction.

2 *STEREO*/HI-1A INSTRUMENTATION AND DATA PREPARATION

The Heliospheric Imager on the *STEREO*-Ahead spacecraft (HI-1A) provided the data for the large-scale analysis. A summary of the data analysis pipeline is given in the Appendix. This instrument is described in detail in Eyles et al. (2009) but for convenience a summary is given here. The HI-1A has a field of view of 20 degrees **by 20 degrees** and is centred on a point 14 degrees away from the centre of the Sun, where the solar F-corona is the dominant large-scale structure. The aperture of the HI-1A lens system is 16 mm, with a focal length of 78 mm. The CCD has a pixel size such that the plate scale becomes 35 arcsec on a 2048x2048 chip, with images binned 2x2 on-board, resulting in 1024x1024 images being returned

with an image bin size of 70 arcsec. A filter limits the spectral bandpass to 630-730 nm with some contribution around 400 nm and 950 nm. The characteristics of the CCD on the HI-1B are similar, with only slight differences in the spectral bandpass (Eyles et al. 2009). Each image is the result of 30 summed exposures, each of 40 seconds, with one image produced every 40 minutes. This prevents saturation by cosmic rays, although planetary and cometary incursions do cause saturation, and also allows for very faint structures in Coronal Mass Ejections (CMEs) and the solar environment to be detected. Stars down to 12th magnitude are detectable and about 650000 stars have been recorded with listed magnitudes brighter than 11.5, with almost 75000 of these being brighter than magnitude 9.5 (Figure 1). Only the very brightest stars, those brighter than about 3rd magnitude, saturate the detector but useful lightcurves can nevertheless still be extracted. Since these stars are mostly within 20 degrees of the ecliptic plane, *STEREO*/HI-1A and HI-1B are therefore searching a region of the sky not well observed by dedicated exoplanet searches, such as *CoRoT* (Auvergne, M. et al. 2009) (**V magnitudes from 11 to 16**), *Kepler* (Koch et al. 2010) (**R magnitudes from 7 to 17**) and SuperWASP (Pollacco et al. 2006) (**V magnitudes from 9 to 13**), and it is also able to view much brighter stars than are normally observed.

Before the data from *STEREO*/HI-1A and HI-1B can be analysed, it must be passed through a pipeline (shown in the Appendix, Figure B1) in order to

- Make a shutterless correction (Eyles et al. 2009)
- Apply a large-scale flat field (Bewsher et al. 2010)
- Apply the pointing calibration to determine the positions of stars (Brown et al. 2009)
- Flag out saturated pixels/columns and missing data blocks (Eyles et al. 2009)
- Carry out a daily background subtraction

2.1 Shutterless correction

The *STEREO*/HI-1A and HI-1B cameras have no shutter and remain exposed during the readout process and also during the clear process prior to each exposure. Consequently, the top of the image is exposed for longer than the bottom of the image, resulting in image smearing during readout. The effect of this can be expressed as a matrix relationship and a correction for the effects of the shutterless operation can be made by a matrix multiplication. If saturation occurs anywhere in a column, then the signal in the affected pixels cannot be corrected in this way and the entire column is flagged as bad data. Further details can be found in Eyles et al. (2009).

2.2 Flat fields

The sensitivity of the *STEREO*/HI-1A and HI-1B cameras varies spatially in three distinct ways. Firstly, the optical properties mean that the solid angle corresponding to each pixel may vary across the field of view, leading to large variations in scale across the CCD. Secondly, the sensitivity of the CCD varies for individual pixels, independently of the sensitivity of adjacent pixels. Thirdly, debris and manufacturing variations and defects on the CCD generate variations in sensitivity over the scale of tens to hundreds of pixels.

It is unknown to what extent the sensitivity of the CCD will vary over time but it is anticipated that the largely stationary F-corona in the field of view may be enough to cause some degradation. The flat field calibration is updated on a regular basis, however, which should prevent this becoming a problem.

The flat field calibrations are performed on *STEREO*/HI-1A and HI-1B images after the removal of the CCD DC bias (Eyles et al. 2009) and the application of the shutterless correction.

Images with significant optical ghosts due to saturated objects in the data are not used for flat fielding. The methodology is detailed in full in Bewsher et al. (2010). Observations of stars near a region of the frame close to the edge of the solar disk are discarded due to additional noise of solar origin.

2.3 Pointing calibration

Calibrated instrument pointing solutions have been derived by comparing the locations of stars identified in the *STEREO*/HI-1A and HI-1B images with known star positions given in the NOMAD astrometric dataset (Zacharias et al. 2004). In the raw (L0.5) data, nominal pointing information is provided, however once the data has been processed to L1 (by running *secchi_prep*) the calibrated pointing information is provided. Full details on the calibration and pointing procedure can be found in Brown et al. (2009).

For the *STEREO*/HI-1A and HI-1B cameras, the average root mean square distance between stars as seen in the image and the location given in the catalogue is about 0.1 pixels, i.e. 7 arcsec. Thus any pointing offsets have a negligible effect on the efficacy of the stellar lightcurves.

2.4 Photometric calibration

The methodology used to determine the photometric calibration is described in full in Bewsher et al. (2010), which includes more up-to-date flat fields and calibration constants than were available for the analysis presented in this paper. Aperture photometry of well-isolated stars down to 12th magnitude is used, that have no other stars with a difference of ≤ 1 magnitude within 1000 arcsec.

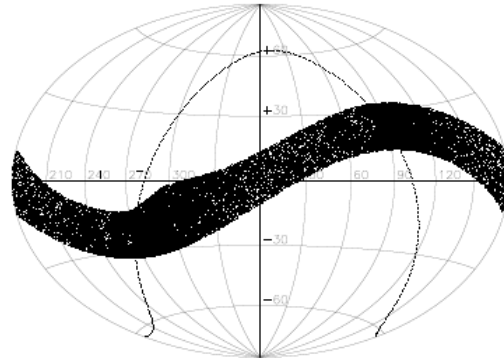


Figure 1. The locations of stars in the *STEREO*/HI-1A with measured mean magnitude of 9th magnitude and brighter.

Whilst future large-scale analyses will use the most up-to-date calibration of Bewsher et al. (2010), the photometric calibration of the *STEREO*/HI-1A used in the analysis presented herein is described by the following formula

$$\text{STEREO magnitude} = d \log\left(\frac{\text{counts}}{c}\right) \quad (1)$$

where $d = -2.49501$ and $c = 18337.7$ for *STEREO*/HI-1A for a 3.5 pixel radius aperture. The number of counts is expressed as a flux intensity in units in data numbers, DN s^{-1} as provided by *secchi_prep*. For analysing HI-1B, the following formula is used (explained more fully in Bewsher et al. (2010))

$$\text{STEREO magnitude} = d \log\left(\frac{a * \text{counts}}{b * c}\right) \quad (2)$$

where $d = -2.5$, $a = 4$ is a correction factor, $b = 0.98$ and $c = 97026$ are the calibration constants for *STEREO*/HI-1B for a 3.5 pixel radius aperture.

3 DATA ANALYSIS PIPELINE AND METHODS

Three methods were used to quantify the variability of each star in the *STEREO*/HI-1A database with a magnitude of 10.5 or greater, thus eliminating the faintest stars with the lowest signal-to-noise ratio (Figure 1 shows the locations of stars with measured mean magnitude of 9th magnitude and brighter with more than twenty photometric points on their lightcurve). They were: the Box-Least-Squares (BLS) (Kovács et al. 2002), the Lomb-Scargle periodogram (Scargle 1982) and Stetson's variability index (Welch & Stetson 1993). IDL code to produce a Lomb-Scargle periodogram was obtained from Armagh Observatory, whilst the others were custom implementations. Figure 2 shows the steps in the analysis as produced by the programs doing the analysis.

Before being passed to the algorithms for analysis, a 7th order polynomial fit was carried out for each lightcurve to remove both natural and artificial trends that might obscure the faintest transit signals (the top two graphs of Figure 2 show an example lightcurve before and after this polynomial detrending). It should be emphasized that whether or not there is genuine long term variability that would be removed by this is not a concern as the focus is on recovering eclipsing variables and exoplanet transits whilst retaining the capacity to detect other short term variables, such as RR Lyrae and δ Scuti stars. The IDL built-in routine `poly_fit` was the basis of this. Each lightcurve was then passed through a combined low and high pass filter in an attempt to remove some remaining noise. This was done by transforming into the frequency domain using the IDL built-in routine `fft` and applying a mask that blocked all features within one standard deviation of the mean before using the inverse transform to return to the time domain. This process was repeated for each epoch of observations for each star and each epoch was analysed separately by the different algorithms (The third graph in Figure 2 shows the BLS spectrum). The strongest signals found from analysing all the epochs for each star were recorded and stored in an output file associated with each field of view, as were a variety of other statistics (q.v. Section B).

The reasons for processing each epoch separately are the presence of noise and artefact features that exist within one or more epochs but seldom all, such as a planetary incursion into the field of view by Venus or Mercury, the existence of some features near the beginning or end of some epochs as a result of streamers or other solar activity and the presence of occasional de-pointing events, typically from micrometeorite impacts, all of which would produce a false signal if all epochs were analysed together. As the highest values from all epochs are stored, these features still give some false signals but by analysing data from unaffected epochs a genuine value may sometimes supersede the false one. Nevertheless, the severity of some noise and artefacts precludes detection of faint signals, which is only partially alleviated in some cases by a direct visual inspection of lightcurves for signs of genuine variability.

Once a star had been identified as an eclipsing binary candidate on the basis of the statistics generated, its detrended, filtered lightcurve and phase-folded lightcurves on the periods of the strongest signals found by the BLS and Lomb-Scargle analysis were examined visually to determine if the variability detected was likely to be genuine. An initial classification of the type of variability was made at this stage. Those that were considered likely to be eclipsing binaries were imported into the software package PERANSO (Vanmunster 2008) for more detailed analysis. There is the possibility that many contact binary systems might have been excluded at this stage due to an inability to distinguish between different types of variability. Indeed, there is some evidence that a significant number of

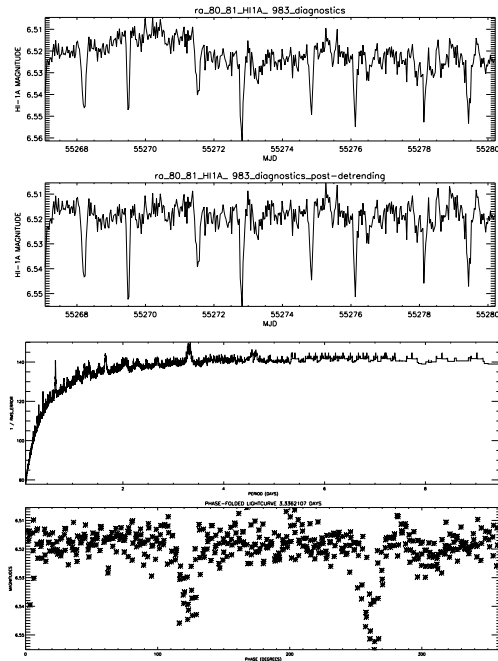


Figure 2. The main stages of the detrending and analysis, demonstrated by the star HR 1750. Starting with the top graph showing the raw light curve for one epoch of observations, the next graph down shows the results of detrending with a 7th order polynomial, the **third graph shows the periodogram derived from the detrended lightcurve and the bottom graph is the lightcurve phase-folded on the period of the strongest signal found from the periodogram.** Note that it is unknown whether the trend removed by the polynomial fitting is artificial or genuine variability - this potential long term variability is not the type of variability being searched for.

fainter contact binaries may have been excluded in this manner (**Section 6**).

Within PERANSO, a detailed analysis of the BLS spectrum would be used to establish as accurate a period as possible using as many epochs as possible, using the software's ability to manually exclude observation points that are likely to be noise or artefacts. The lightcurve phase-folded from this period would be used to finally determine if the star was likely to be an eclipsing binary. If it was still considered an eclipsing binary, the phase-folded lightcurve would provide estimates of the primary eclipse depth and minimum eccentricity. The minimum eccentricity would be estimated by visually determining the offset of secondary eclipses, where these could be distinguished as such, from a phase of 0.5 away from the primary eclipse. The estimated errors in the estimate were taken as the extremes of the possible ranges of where the secondary minimum might be, thus the errors are larger for smoother, shallower eclipses as in many contact binaries. The values ob-

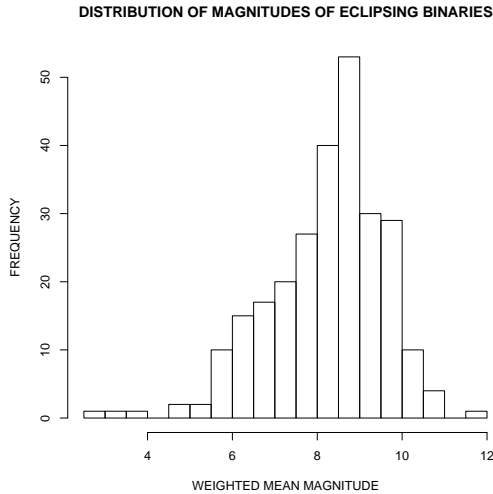


Figure 3. The distribution of the 263 eclipsing binaries observed by *STEREO*/HI-1A by weighted mean magnitude. The fall-off after magnitude 9 is the result of the decreasing signal quality with magnitude increasingly preventing the detection of eclipse signatures.

tained were then, along with the errors, multiplied by two, giving a value that is actually $|e \times \cos \omega|$ or effectively a minimum eccentricity that could be significantly higher depending on the value of ω , the argument of periastron.

The values of the period, primary eclipse depth and $|e \times \cos \omega|$ found from this detailed examination were recorded, along with the output of the different algorithms, the star’s Celestial co-ordinates, its identity (from SIMBAD) and spectral type (from SIMBAD) as well as the identity of any nearby star (within 6 arc-minutes, from SIMBAD) that could potentially have contaminated the signal and whether or not either the star or this neighbour had previously been identified as an eclipsing binary. This dataset of 263 eclipsing binaries (Table B1) was then explored for interesting trends and patterns.

3.1 Trends

The distributions of the recorded characteristics show some trends that apply to the sample as a whole. Most significantly, the distribution of eclipsing binaries by weighted mean magnitude (Figure 3) shows a peak between magnitude 8.5 and 9.0 after which the numbers extracted fall off. This implies that, due to a combination of sensitivity and noise, eclipses are not being detected around fainter stars since the distribution of eclipsing binaries is expected to match the distribution of stars in the database, the numbers of which continue to increase with increasing magnitude.

The periods given in the statistics are the primary-to-

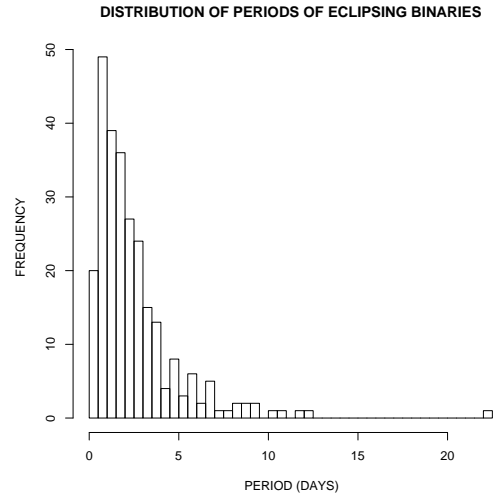


Figure 4. The distribution of the 263 eclipsing binaries observed by *STEREO*/HI-1A by period.

primary period, although difficulty in distinguishing primary from secondary eclipses may cause the resulting value to be out by a factor of 2. The distribution of the periods of the eclipsing binaries extracted reflects, as expected, the bias due to the length of individual epochs (Figure 4). In order to get a good signal, three transits must be observed within an epoch and thus there is a tendency to find periods of less than this threshold. Through the presence of secondary eclipses longer periods can be found but visual examination is required for detecting the very longest period eclipsing binaries, especially if the system is eccentric. The star with the longest period confirmed of the 263 is HD 72208 with 22.013 days (see Section 4 for details), which cannot be found through a separate analysis of each epoch but only through all three epochs presently available, owing to the significant eccentricity ($|e \times \cos \omega| = 0.391 \pm 0.006$) and the fact that no more than two transits are observed in any epoch. There is a suspected eclipsing binary with a potentially longer period showing only one primary eclipse in each epoch (HD 173770, see Section 4) but a definite period determination cannot be made and it was not included in the sample.

The distribution of the depths of primary eclipses reveals a trend that is interpreted as the presence of different populations of eclipsing binary (Figure 5). Only **detached and semi-detached EBs** appear to have a primary eclipse depth greater than 0.5 magnitudes, whereas contact binaries predominate at depths of 0.3 magnitudes and below.

The estimates of $|e \times \cos \omega|$ reveal that 24 of the 263 eclipsing binaries have measurable eccentricity (see the Appendix for their phase-folded lightcurves). Other EBs in the

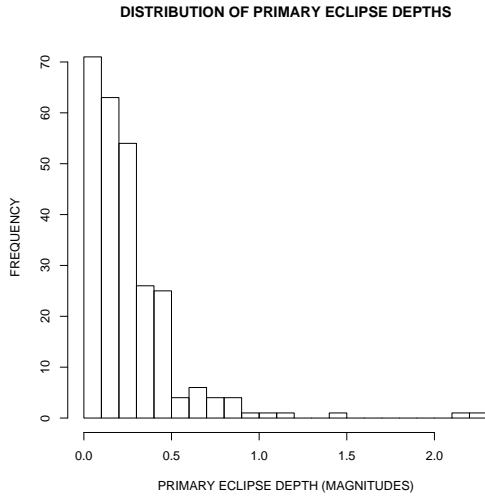


Figure 5. The distribution of the 263 eclipsing binaries observed by *STEREO*/HI-1A by primary eclipse depth.

sample may have eccentricity, as the value of the argument of periastron, ω , is unknown and there are some that show a hint of eccentricity but the margin of error does not preclude the possibility that they might have zero eccentricity, including a couple that are exactly on the line where the error margin equals the estimate of $|e \times \cos \omega|$. Thus a small but significant fraction of the sample are eccentric, with more than 5% showing significant eccentricity. The sample of eccentric systems is not quite large enough to show statistically valid trends, unfortunately, although the indications are that small eccentricities dominate with larger eccentricities being widely distributed. Nevertheless, this result is broadly in agreement with recent findings from the *Kepler* mission (Prsa et al. 2010), however the sample of stars observed by *STEREO*/HI-1A is not limited to main sequence stars or by other selection criteria intended to maximise the chances of finding an exoplanet transit. It is therefore a useful result that it appears to find a similar distribution of $|e \times \cos \omega|$ to the *Kepler* sample as it implies that eccentricity is not dependent upon spectral type. Eccentric systems are expected to circularise over time and thus these systems are much-studied in the field of stellar evolution to model interactions between multiple stars as an interaction with a third body is usually required for them to be formed (Claret & Willems 2002).

The distribution of spectral types of the eclipsing binary primary stars shows a predominance of younger, hotter stars of earlier spectral types (Figure 8). The main limitation of this distribution is that the spectral type of the closest star to the co-ordinates of the perceived eclipsing binary may not always be the star that is actually eclipsing, due to the low spatial

DISTRIBUTION OF ECCENTRICITIES WITH ERROR MEASUREMENT

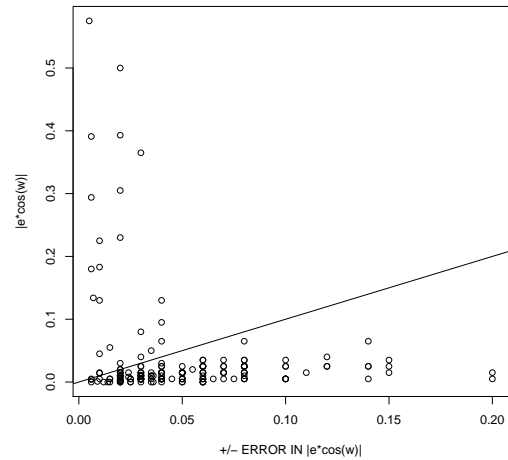


Figure 6. The estimates of the minimum eccentricities ($|e \times \cos \omega|$) of the 263 eclipsing binaries observed by *STEREO*/HI-1A, where measurable, against the errors for each measurement. Each open circle represents a single eclipsing binary. Those points above the line represent eclipsing binaries for which an eccentricity of zero is outside the range of the errors in the measurement.

DISTRIBUTION OF ECCENTRICITIES AS $|e \times \cos \omega|$

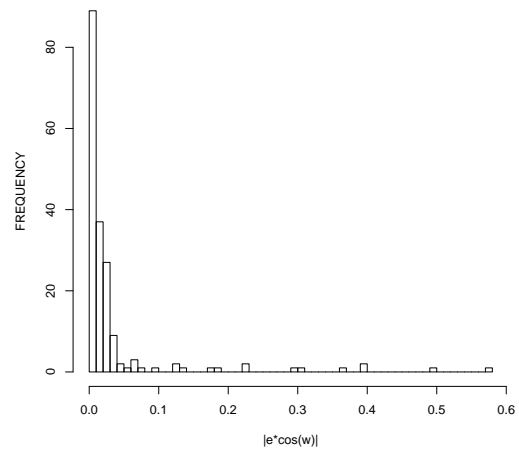


Figure 7. The estimates of the minimum eccentricities ($|e \times \cos \omega|$) of the 263 eclipsing binaries observed by *STEREO*/HI-1A, where measurable.

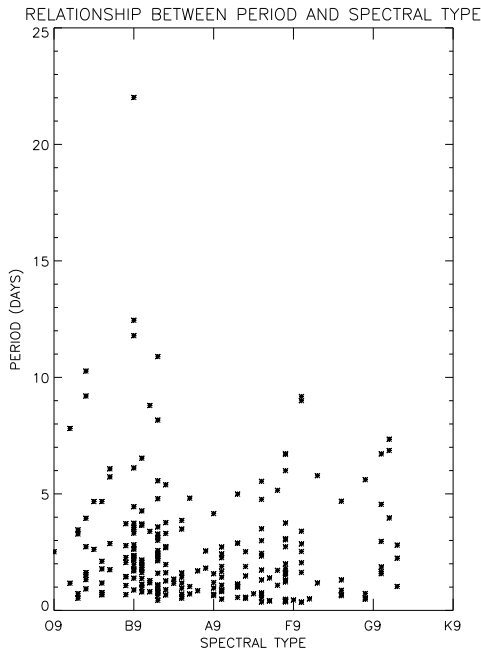


Figure 8. The 232 eclipsing binaries observed by *STEREO*/HI-1A with a known spectral type, showing the relationship between spectral type and period. **The most common spectral type is A2, with 22 stars in the sample.** There are no clear patterns connecting the spectral type with period, however there are some cases where the specific star causing the eclipses has not been identified and the spectral type is of the star closest to the target co-ordinates (see Appendix A).

resolution and the possible contamination of lightcurves by nearby stars. The distribution will also be affected by any bias in the *STEREO*/HI-1A database, with only stars brighter than magnitude 10.5 being analysed en masse (although one or two fainter examples were identified visually).

The distribution of eclipsing binaries by their signal detection efficiency (SDE) from the BLS algorithm (Figure 9) shows two indistinct peaks, interpreted as corresponding to two different types of eclipsing binary. The peak with the highest SDE corresponds mostly to detached binaries, whose lightcurves are a closer match to the box-like shape the BLS algorithm checks for. The broader peak with the lower SDE corresponds to contact binaries, which have smoother, more sinusoidal lightcurves. An Algol type binary might be the highest-rated by the BLS algorithm in its field but contact binaries can sometimes be near the bottom of such a list and thus are not reliably detected by this algorithm. The Lomb-Scargle periodogram, (distribution shown in Figure 10), preferentially reveals contact binaries, although it typically does give a signal for many detached binaries as well, albeit increasingly less

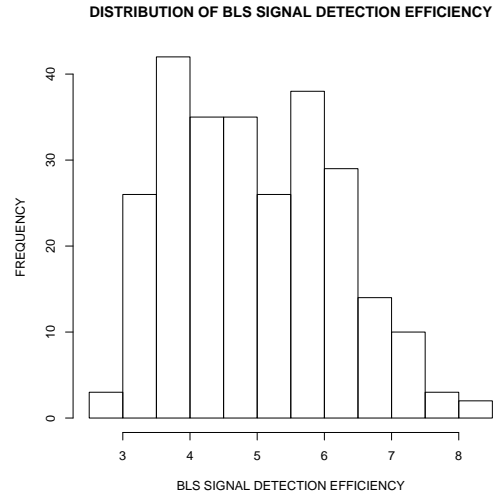


Figure 9. The distribution of the 263 eclipsing binaries observed by *STEREO*/HI-1A by BLS signal detection efficiency.

so for shallower, more box-like eclipses (Figure 11). Combining the BLS and the Lomb-Scargle methods thus produces a positive signal for the vast majority of the eclipsing binaries, with those rated poorly by both being stars with fewer data points (both algorithms give higher scores for more data points, thus stars with less data available are rated less highly), those with very long periods and those with comparatively low signal-to-noise that were detected by visual examination.

The effect of the period on the output of the BLS and Lomb-Scargle methods was also investigated (Figures 12 and 13). The dependence discovered is again likely representative of the shape of the transits.

As a variety of noise signatures were encountered in the dataset, some very clearly obscuring genuine signals, producing both false positives and false negatives, an attempt to evaluate the effects of noise was made (Figures 14, 15, 16 and 17). Together these appear to show a tendency to overlook shallow eclipses. This may be partly due to a mixture of red and white noise and also due to problems classifying contact binaries as such when their **lightcurves are not clear enough to distinguish them from sinusoidal variations. Blending also has a tendency to obscure faint signals, with the brightest object in the photometric aperture dominating but showing additional signals overlaid, or with stars of similar magnitudes showing constructive or destructive interference resembling an amplitude modulation. This has the effect of lowering, broadening and sometimes splitting peaks in a periodogram analysis, which affects the ability of an algorithm to identify a low-amplitude signal.**

Since a large proportion of the sample of eclipsing bi-

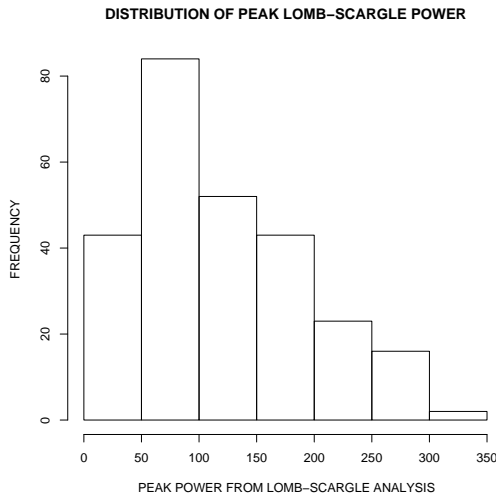


Figure 10. The distribution of the 263 eclipsing binaries observed by *STEREO*/HI-1A by peak power from a Lomb-Scargle periodogram analysis.

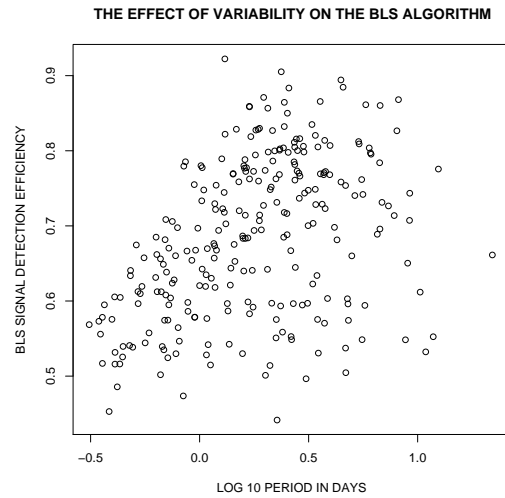


Figure 12. The dependence of the BLS algorithm on the period of a signal. The influence is believed to be the shape of the light curves of variables with increasingly short periods, rather than the period itself. Each open circle represents a single eclipsing binary.

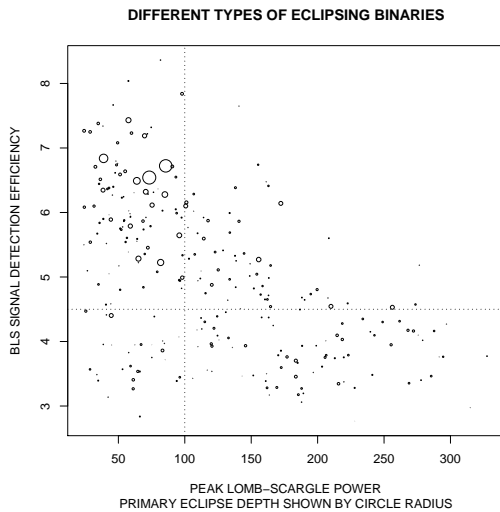


Figure 11. Comparison of the ability of the BLS and Lomb-Scargle algorithms to extract the signals of eclipsing binaries. Each eclipsing binary is represented by a circle with a radius proportional to the depth of the primary eclipse. Points above the horizontal line have a SDE high enough to be considered a detection by the BLS algorithm, whilst those to the right of the vertical line may similarly be considered to have been detected by the Lomb-Scargle algorithm, in the absence of artefacts and noise producing large numbers of similar signals. Those rated poorly by both were typically found through visual examination.

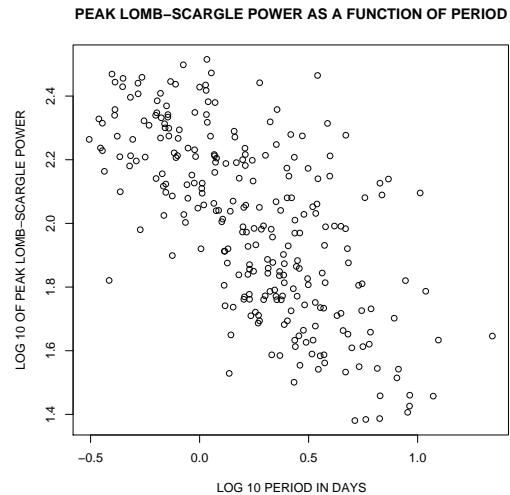


Figure 13. The dependence of the Lomb-Scargle method on the period of a signal. Each open circle represents a single eclipsing binary.

aries appear to be previously undetected or, at least, unconfirmed as such by previous observations, a search was made for characteristics in common to understand what, if anything, might be different about the new cases that might explain why they had previously gone undetected (Figures 18). As might be expected, there is a tendency for the new cases to have shall-

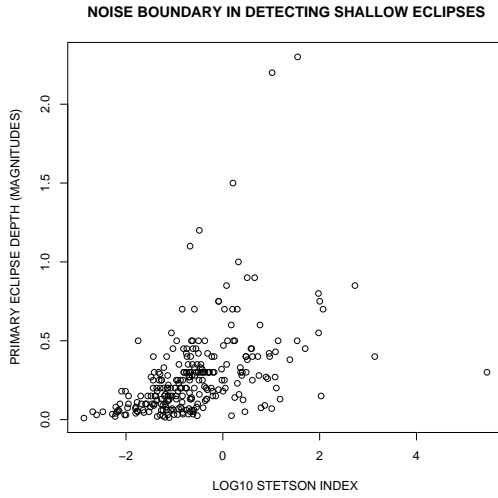


Figure 14. The dependence of primary eclipse depth on the Stetson index. The sharp cut-off at about -0.5 shows that eclipses with a primary eclipse depth less than 0.3 magnitudes are considerably more difficult to detect through noise or variability. Each open circle represents a single eclipsing binary.

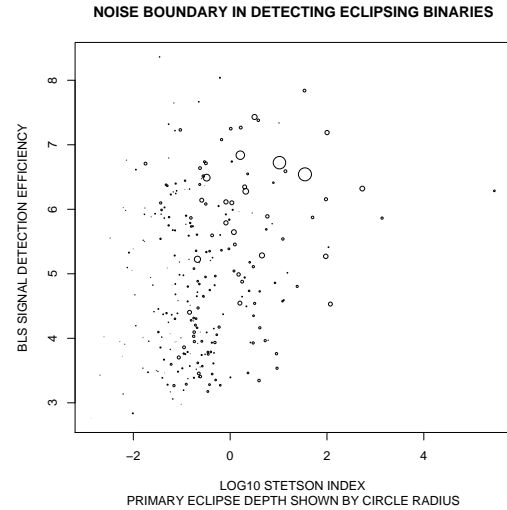


Figure 16. The dependence of signal detection efficiency as a function of Stetson index. The cut-off point at about -0.5 shows that variability or noise above a certain level is obscuring the signals of some eclipsing binaries, although the apparent clustering of signals around a moderate value and especially the higher ratings for deeper eclipses shows that the Stetson index is also to some extent reflecting the variability due to eclipses. Each eclipsing binary is represented by a circle with a radius proportional to the depth of the primary eclipse.

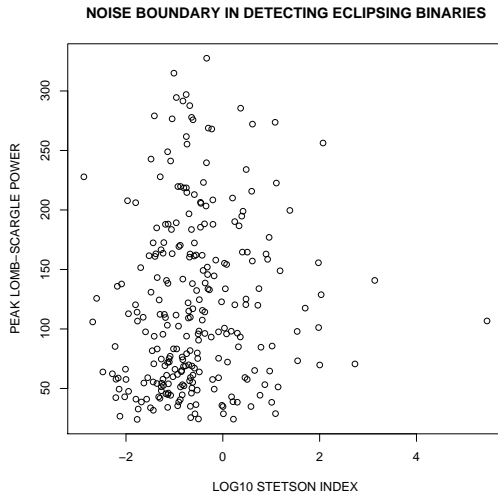


Figure 15. The dependence of peak power from a Lomb-Scargle periodogram analysis as a function of Stetson index. The cut-off point at about -0.5 shows that variability or noise above a certain level is very effective at obscuring the signals of eclipsing binaries, regardless of their peak power. Each open circle represents a single eclipsing binary.

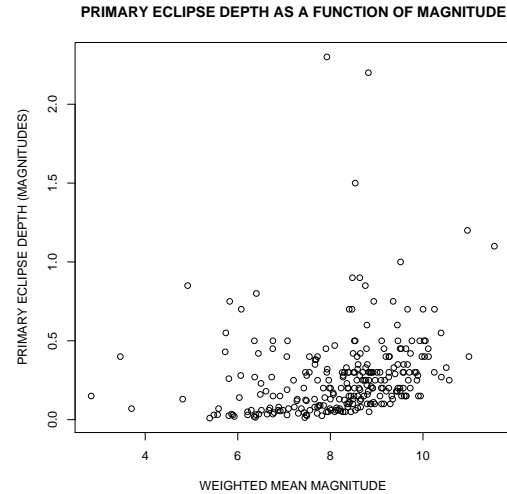


Figure 17. The dependence of primary eclipse depth as a function of weighted mean magnitude. After about magnitude 8.5 shallower eclipses are not detected, with the threshold rising nearly linearly. Each open circle represents a single eclipsing binary.

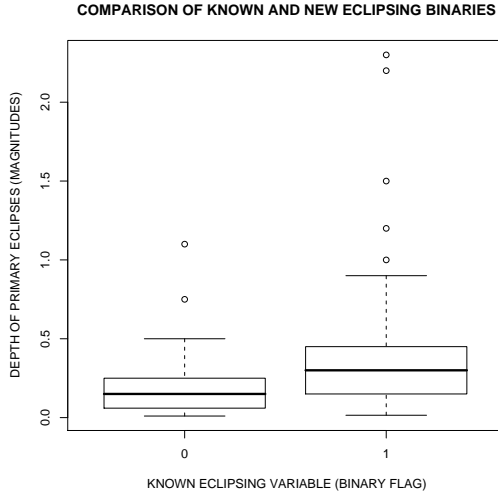


Figure 18. Comparison of the distribution of known and new eclipsing binaries with respect to the depth of their primary eclipses. The tendency of the newly-discovered systems to show fainter eclipses reflects both the sensitivity of the *STEREO*/HI-1A and the expected bias of previous surveys in discovering deeper eclipses. The centre box contains those EBs in the second and third quartiles with the median represented by a thick line within, whilst the outer bars represent an approximately 95% confidence level and outliers are individual open circles.

lower eclipses than those previously known. There does not appear to be any significant difference in either the periods or magnitudes found, however.

A previously known tendency for eclipsing binaries with long periods to be more likely to be eccentric (Mathieu & Mazeh 1988) is confirmed by the *STEREO*/HI-1A observations (Figure 19).

To summarise briefly, the BLS is the algorithm of choice for extracting box-like eclipses, e.g. Algol binaries or exoplanet transits. The Lomb-Scargle algorithm is best at extracting sinusoidal-like signals but also has some limited capability to extract other regular signals. The Stetson index is able to extract large amplitude variables of all types.

4 RESULTS

Of the 263 eclipsing binaries extracted, 122 are not recorded as such in SIMBAD. Some of these are, however, known variables of other types or are suspected of variability. Owing to the purely photometric data available from *STEREO*/HI-1A, there remains the possibility of mis-classification, however care was taken to include only stars whose phase-folded lightcurves appeared to be clear cases. Thanks to the excel-

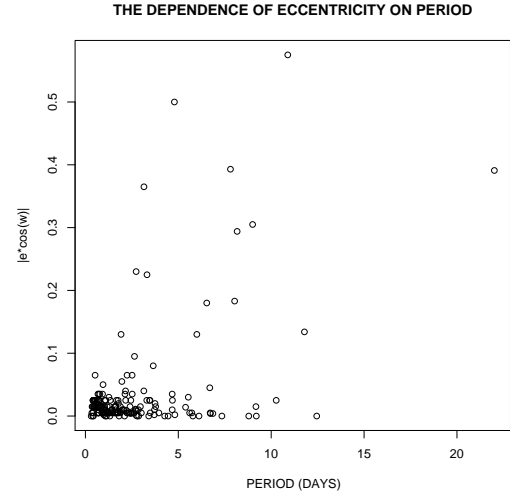


Figure 19. The dependence of the minimum eccentricity of the 263 eclipsing binaries observed by *STEREO*/HI-1A, as measured by $|e \times \cos \omega|$, on the period of eclipses. Each open circle represents a single eclipsing binary.

lent phase coverage resulting from the *STEREO*/HI-1A observational cadence of 40 minutes maintained for up to 19.44 days, with three or four such epochs for most stars, the new observations are in many cases clearer than those previously available and in some cases the existing classification may be in need of revision. A total of 24 of the eclipsing binaries have measurable eccentricity and their lightcurves are shown in the Appendix (Figure B2).

4.1 Individual stars of interest

4.1.1 HD 213597: substellar transit candidate

The best potentially substellar transiting candidate is HD 213597. This star is recorded in SIMBAD as being of spectral type F0 and is not suspected of any variability. The observed eclipses are box-like, with very sudden ingress and egress phases, and are uniformly about 25 mmag deep, with a period of 2.4238 days between successive eclipses (Figure 20). Secondary eclipses are not evident.

4.1.2 V 471 Tau: cataclysmic variable progenitor

Although it does not feature in the sample, as the eclipses by the white dwarf secondary are too short to be observed, V471 Tau nevertheless is an important star and the *STEREO* observations in both HI-1A (Figure 22) and HI-1B (Figure 23) have the potential to inform studies of the magnetic activity cycle of the red dwarf primary (eg. O’Brien et al. 2001),

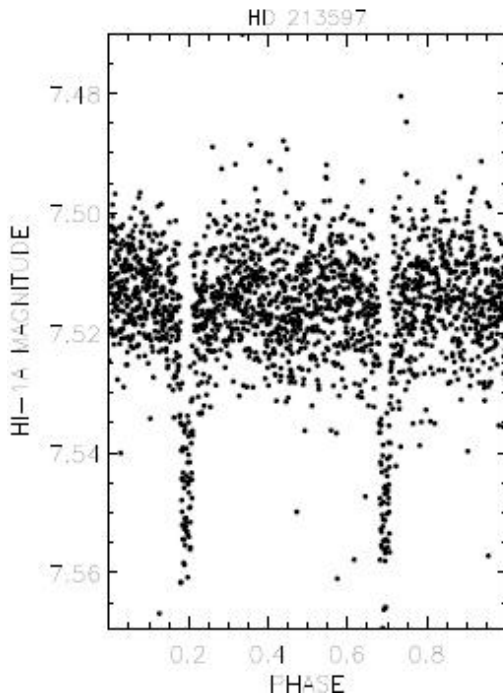


Figure 20. Lightcurve of the star HD 213597, phase-folded on a period of 4.8476 days.

(Hussain et al. 2006) and (Kamiński et al. 2007)). As a cataclysmic variable progenitor, with an unexpectedly massive red dwarf primary and the most massive white dwarf in the Hyades (O’Brien et al. 2001), studies of this star may have a considerable effect on understanding the mechanism behind type Ia supernovae, thereby influencing the calibration of the extragalactic distance scale and much of modern cosmology. Note that the spectral bandpass of the HI-1A and HI-1B imagers both allow a component of blue light through (Bewsher et al. 2010) and the white dwarf secondary is estimated to contribute 6 % of the flux in this part of the spectrum (O’Brien et al. 2001). Similar behaviour can be seen in *STEREO* observations of RS CVn variables, e.g. SZ Psc, and shows that *STEREO* is a useful resource for studies of similar variability that require photometry with both long and short baselines.

4.1.3 Highly eccentric eclipsing binaries

The most eccentric undiscovered eclipsing binary in the sample is HIP 92307, with $|e \times \cos \omega| = 0.500 \pm 0.020$ (Figure 24). Both primary and secondary eclipses are about 30 mmag deep, indeed it is not clear which are the primary and secondary eclipses. This star is listed as spectral type A2V.

The longest period eclipsing binary in the sample is

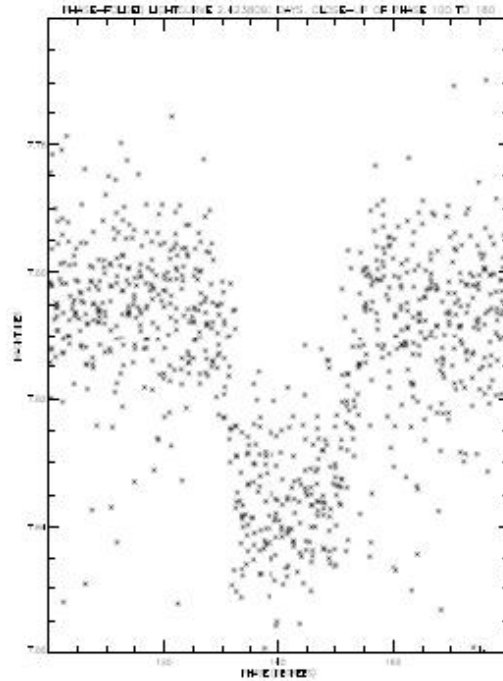


Figure 21. Close-up of the transit of HD 213597, phase-folded on a period of 2.4238 days. This lightcurve was constructed using the latest data available, including updated flat-fields as well as data from *STEREO*/HI-1B.

HD 72208, with 22.0130 days between primary eclipses and $|e \times \cos \omega| = 0.391 \pm 0.006$, making it one of the more eccentric as well (Figure 25). This star, spectral type B9p, is a spectroscopic binary. Both primary and secondary eclipses are about 60 mmag deep.

Possibly the longest period eclipsing binary so far observed in the *STEREO*/HI-1A data may be HD 173770. As there are multiple possible periods that can fit the lightcurve, it was not included in the sample. The best-fitting period that has been found with the data available shows a period of 25.145 days, which implies a minimum eccentricity $|e \times \cos \omega| = 0.108 \pm 0.012$. The star shows some intrinsic regular variability as well, although the exact type has not been classified. The host star is listed in SIMBAD as being of spectral type B6V and is a suspected triple system. With the separation given for these components, it is unlikely either are responsible for the eclipses and this may instead be a quadruple system. The lightcurve is included in Figure B2 for comparison with the other measurably eccentric eclipsing binaries.

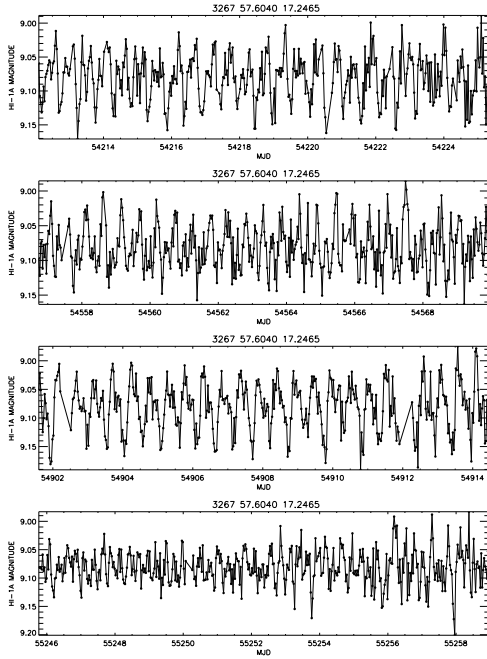


Figure 22. Lightcurve of the star V471 Tau, as observed by the *STEREO* HI-1A imager. 3267 is the catalogue number of the star in the *STEREO* HI-1A field of view for right ascension: 50-60 degrees and declination: 10-20 degrees.

4.1.4 NSV 7359: β Cepheid showing the Kozai effect

A well-observed bright star, NSV 7359 shows relatively deep eclipses with a period of 9.1999 days that have not been recorded in SIMBAD (Figure 26). This star is a known β Cepheid, with an amplitude listed as 30 mmag. Given the volume of observations, it is very surprising this variability has not previously been recorded. It is in a fairly crowded area with many stars close by in the *STEREO*/HI-1A field of view, yet none of these are sufficiently bright to contaminate its lightcurve to the extent of eclipses as deep as those observed. The eclipses are therefore genuine and should help to further inform the parameters previously determined for this star. Interestingly, this star is also shown in SIMBAD to be a spectroscopic binary with a period of 0.2872 days, which would mean the eclipsing companion is a tertiary component and not the secondary. The Kozai effect (Kozai 1962) may have caused the inclination of the system to change so that eclipses are now visible.

4.1.5 HR 7355: rotational variable or contact binary?

One of the better-observed stars in the sample is HR 7355 (a.k.a. HIP 95408 and HD 182180). *STEREO*/HI-1A shows

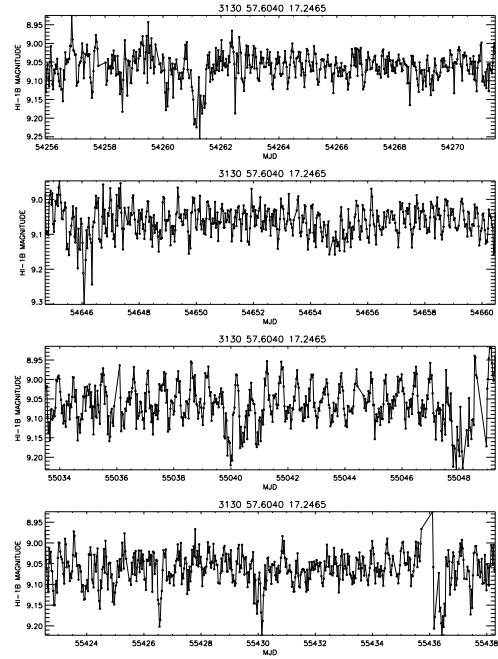


Figure 23. Lightcurve of the star V471 Tau, as observed by the *STEREO* HI-1B imager. 3130 is the catalogue number of the star in the *STEREO* HI-1B field of view for right ascension: 50-60 degrees and declination: 10-20 degrees. The scale of the y-axis has been adjusted to fit the data range.

what appears to be a clear-cut case for an eclipsing binary as the phase-folding on 0.5214 days indicates in Figure 27. Other studies have noted this periodicity and associated it with a rotation period, however, rather than attributing it to a secondary companion, even the most recent which show the variability to be eclipse-like (Oksala et al. 2010). We suggest that the photometry from *STEREO* is enough to warrant a re-appraisal of the nature of this system. It has been left in the sample as an eclipsing binary since from the photometry alone that is what it appears to be. In the wider context it is clearly an unusual and fascinating, chemically peculiar star that continues to attract further study.

4.2 False positives

A small number of stars showing variability on a similar scale to that expected of an exoplanet or brown dwarf transit could be ruled out as such from photometric data alone, or in combination with other information known about the host star.

Total eclipses just 30mmag deep were observed around either HIP 248 or HIP 247 (near-identical signals and in the same or adjacent pixels in *STEREO*/HI-

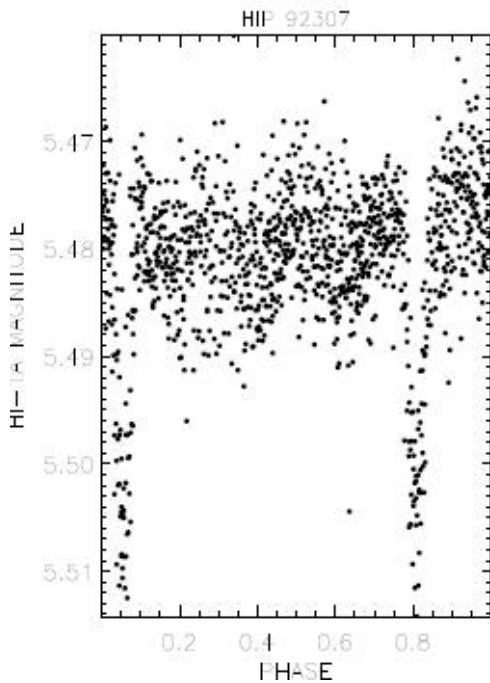


Figure 24. Lightcurve of the star HIP 92307, phase-folded on a period of 4.7911 days. $|e \times \cos \omega| = 0.500 \pm 0.020$.

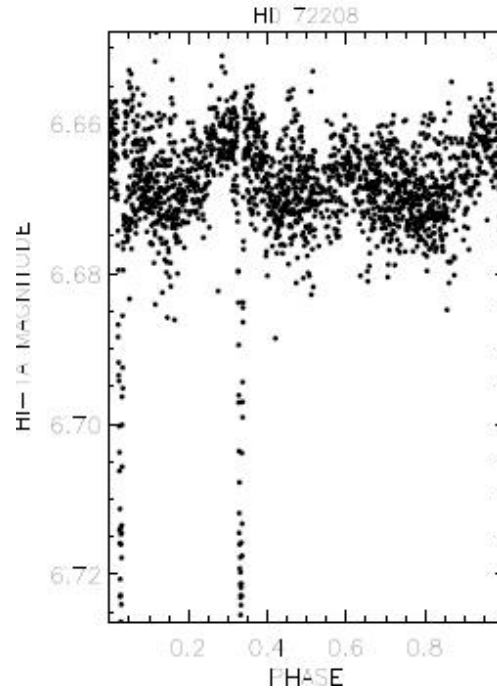


Figure 25. Lightcurve of the star HD 72208, phase-folded on a period of 22.0130 days. $|e \times \cos \omega| = 0.391 \pm 0.006$.

1A). These stars are both of spectral type F0, however the eclipses include a substantial amount of time in the ingress and egress phases. The eclipses are consistently about 30 mmag deep and 2.2604 days apart (Figure 21). This is a transit by a larger, stellar body rather than a brown dwarf but a low-mass star remains a possibility.

The star HD 222891 has similar features to HIP 248, however the eclipses are also too deep, at 40 mmag, with the host star of spectral type F8, to be due to a brown dwarf companion. It may nevertheless be a low-mass star of some interest.

Of all eclipse-like features extracted from the STEREO/HI-1A database, the shallowest primary eclipses were 7 mmag deep around the star 18 Sgr. This lightcurve appears more like a contact binary, although the raw lightcurve is also somewhat irregular and the behaviour might instead be due to rotational microvariability. It was not considered conclusive enough to be labelled as an eclipsing binary and does not feature in the sample, although more data may help to clarify the lightcurve and its classification.

NSV 1321 is the most marginal detection in the sample. In order to verify whether the 10 mmag eclipses observed were genuine, differential photometry was carried out, however this appeared to introduce variability from a neighbouring star - it is located in a crowded field with several

stars showing clear variability and others blended. Although the star itself is classified as variable, the NSV catalogue as shown in SIMBAD indicates this variability was considered doubtful by the catalogue's compilers. With the host star of spectral type B8V this would not be an exoplanet signal and is most likely a grazing eclipse or stellar companion. Although the possibility of microvariability or a blend with a neighbouring star cannot be wholly ruled out, none of the neighbouring stars show a periodicity of 2.2663 days so this was included in the sample.

Another star showing shallow eclipses that was ruled out from being a brown dwarf is II Cnc (period from STEREO/HI-1A of 1.0684 days, eclipses 25 mmag deep). This is listed in SIMBAD as a BY Draconis type variable of spectral type G8V, however there is no mention of it showing eclipses. The shape of the lightcurve is indicative of either a contact binary or grazing stellar transits with secondary eclipses present. The period is more representative of a contact binary. The secondary may nevertheless be a low-mass star, making this a relatively unusual system for a contact binary.

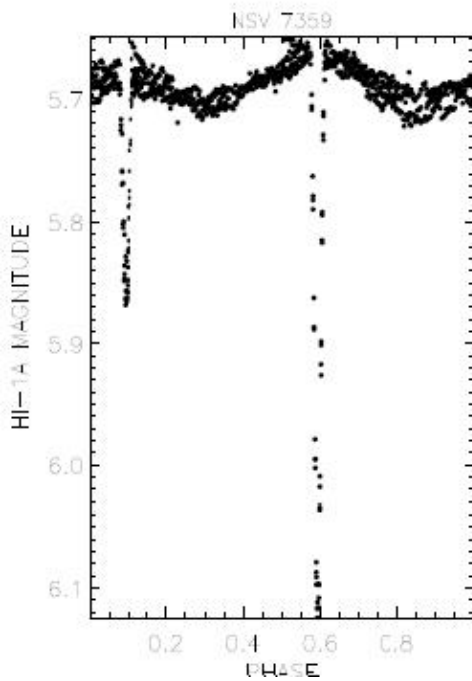


Figure 26. Lightcurve of the star NSV 7359, phase-folded on a period of 9.1999 days.

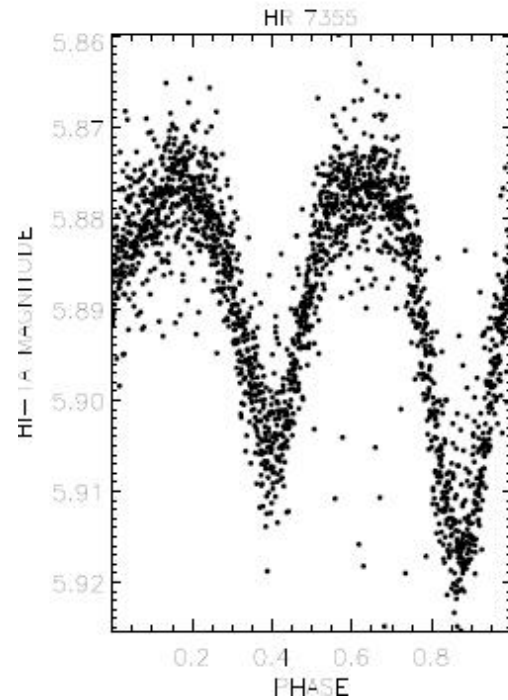


Figure 27. Lightcurve of the star HR 7355, phase-folded on a period of 0.5214 days.

5 SURVEY PROSPECTS

Although the analysis thus far done has been restricted to recovering eclipsing binaries and searching for exoplanets, the prospects for recovering variables of different types has been investigated.

The prospects for exoplanet extraction are summarised in Figure 29 for the declination strips away from the Galactic Plane for the ranges of periods and magnitudes shown. This indicates reasonable prospects for finding a signal, if any exist around stars of about 7th magnitude or brighter but with a sharp fall-off for fainter stars, such that the probability of extraction is negligible for stars fainter than 8th magnitude from *STEREO/HI-1A* data alone. Note that the most significant **substellar candidate so far extracted is magnitude 7.5**. For reference, the signal of HIP 247 and HIP 248 (magnitude 7.5, period 2.2604 days) is 30 mmag deep detected with a significance of 5σ and the 30 mmag deep signal of HR 1750 (magnitude 6.5, period 3.3150 days) is detected with a significance of 8σ . With the inclusion of *STEREO/HI-1B* data the number of data points will more than double (this satellite is in an Earth-trailing orbit and stars remain in the field of view for longer) and the significance of extracted signals will increase, as will the potential for extracting faint signals.

For eclipsing binaries, Figures 14, 17 and 28 indicate that

more may yet be found and Figure 11 shows that the combination of the BLS and Lomb-Scargle methods is a good way of extracting their signals. The difficulty here is that, from photometric data alone, it has not been possible to conclusively classify them as eclipsing binaries. This problem largely affects contact binaries, which have lightcurves that might easily be confused with elliptical variables and short period pulsating stars. The ability of the Lomb-Scargle method to extract contact binaries suggests it would be a useful tool for extracting other variables also.

Asteroseismological studies are likely to require that low-level variability be detected. If a signal of 10 mmag, comparable to an exoplanet transit, is required, then Figure 29 might also be an indicator of the prospects for extracting microvariable behaviour, however this would assume that the algorithm chosen to extract the microvariable signal is equally effective at discerning faint signals as the BLS. Nevertheless, the prospects would appear good for the brighter stars (7th magnitude or brighter) and these are also the most amenable to high-resolution spectroscopic follow-up by other observatories. Investigations of the signals extracted by the Lomb-Scargle method show that the presence of systematic sources of noise inhibits the detection of a test signal, however, so additional cleaning would be required. **Whilst the observ-**

ing cadence of 40 minutes will impair detailed studies of very short period variables, the ongoing examination of the data that is including *STEREO*/HI-1B observations is nevertheless able to obtain very clear photometry from a number of known δ Scuti stars (e.g. DX Cet) and potentially detect new variables down to magnitude 11.

6 CONCLUSIONS

The *STEREO*/HI-1A observations are clearly a valuable resource suitable for a wide range of variability studies. With 263 eclipsing binaries extracted from the database, 122 of which have not previously been identified as such, there is the potential for the discovery of a number of new and interesting objects. The area of the sky being covered and the brightness of the stars being observed are features unique to *STEREO*/HI-1A and simultaneously allow for high quality follow-up observations of interesting objects. There is the potential to discover transiting exoplanets (Figure 29), however this is at the very limit of the survey's sensitivity and would only be possible for the stars with the cleanest signals. A 30 mmag transit around a magnitude 7.5 star is detectable with 5σ significance and a 30 mmag transit of a magnitude 6.5 star is detectable with 8σ significance from *STEREO*/HI-1A data alone. With the inclusion of data from the second satellite, *STEREO*/HI-1B, this will improve, e.g. from *STEREO*/HI-1A data alone the 50 mmag transits of the magnitude 8.5 star BD +03 263p are detected with 7σ significance but with the inclusion of *STEREO*/HI-1B data they are detected with nearly 13σ significance.

The analysis presented here may have some impact on stellar evolution studies, in particular relating to the proportion and distribution of eccentric eclipsing binaries. As the newly-discovered eclipsing binaries are comparatively bright, the masses, radii and effective temperatures can be determined more accurately in follow-up observations and can therefore provide more stringent tests of stellar evolution models (e.g. (Torres et al. 2006), (VandenBerg et al. 2006), (Claret & Willems 2002) and (Stassun et al. 2006)). The new eclipsing binaries will also help to produce more accurate distances to their host stars and any stars those are associated with (Southworth et al. 2005).

The potential to improve upon existing phase coverage, especially relating to that obtained during eclipses, and times of maxima and minima in a variability cycle can help to refine parameters for these important stars. In some cases, the capability of *STEREO* to deliver good photometry over timescales of days and weeks in a single pass, combined with repeated observations after about a year, are ideal for observing long-term changes in variability. This is of particular importance in studies of magnetic activity cycles (eg. V471 Tau) and particular classes of variables, such as RS CVn stars (eg. SZ Psc).

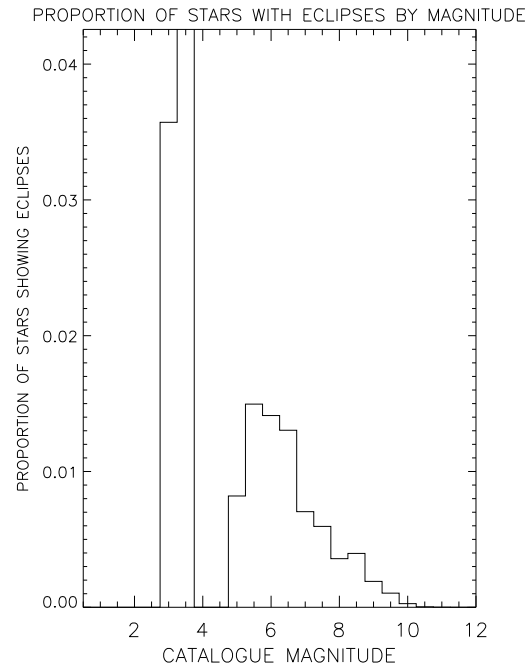


Figure 28. The proportion of stars of different magnitudes that have been found to be eclipsing. **The small number of stars brighter than magnitude 4.5 in the *STEREO*/HI-1A field of view is responsible for the shape at the bright end of this graph, with only three EBs observed.**

The eclipsing binaries newly discovered by this analysis show a tendency to possess shallower transits than those previously known (Figure 18), partly due to the quality and cadence of the photometry. With many of the host stars being of early spectral types, late B and early A, it is possible that many of these systems may be comparatively young (Figure 8). A small but significant proportion are in eccentric orbits (Figures 6 and 7), supporting recent observations by *Kepler* (Prsa et al. 2010). Some particularly interesting systems have been identified for potential follow-up observations, including one good brown dwarf candidate (HD 213597, Figure 20). The proportion of stars of different magnitudes found to be eclipsing indicates that more may yet be found as Figure 28 shows decreasing numbers observed with fainter stars, whereas the real number should be a constant proportion of the population.

Evaluation of the algorithms used to extract eclipsing binaries suggests that, if exoplanets alone are the target, then the **Box-Least-Squares** (BLS) algorithm is capable of effectively extracting them (Figure 29). For a more general search for eclipsing binaries, however, the combination of the BLS along with the Lomb-Scargle periodogram analysis will be required

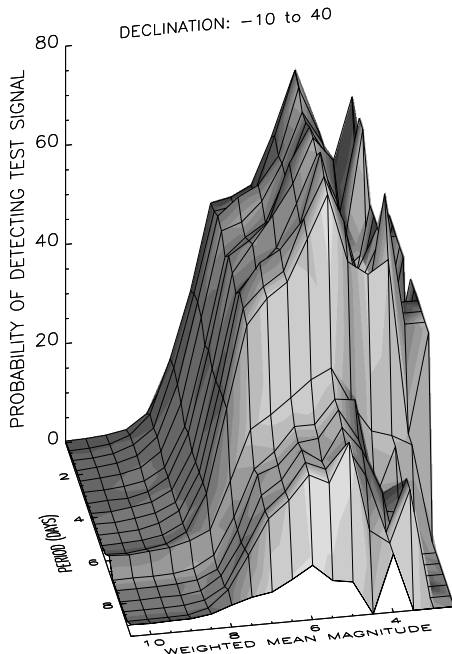


Figure 29. The percentage of stars where a 10 mmag test eclipse superimposed on the real lightcurve was successfully returned as the strongest signal by the BLS algorithm. Each epoch of each star was examined separately and only those that returned the test signal within 0.04 days were considered successes. Detection of a harmonic was not considered a success. This graph thus represents the chance of detecting a transiting ‘Hot Jupiter’ for stars of a given magnitude for the range of periods shown. The stars tested were those with a declination between -10 degrees and 40 degrees and having a weighted mean magnitude within 0.05 magnitudes of the points shown. The trial periods ranged from 0.5 to 9.5 days in half-day steps. The dip in success rates at 6.5 days is the result of many stars having parts of their lightcurve masked out to avoid contamination by solar activity, whilst the dip at 9.5 days is the result of fewer stars remaining in the field of view for long enough for a period of this length to be checked. The small increases in success rates for fainter stars at these periods are due to artificial trends associated with the length of an epoch, which also contributes to an increase in the number of false positives for brighter stars although this number is small compared to the decreases observed for the above reasons. The best **substellar candidate so far extracted has a period of 2.4238 days and a host star of magnitude 7.5: a 25 mmag transit** is detectable with 5σ significance at this level.

in order to extract a high proportion of these objects (Figure 11). The Stetson index can be used as a measure of noise, as well as variability, although it does rate some Algol type binaries very highly so extreme values are not necessarily false positives (Figure 14).

Further research being done includes the development

of a matched filter algorithm and follow-up observations of key targets has begun. A further two eclipsing binaries showing eccentricity have been discovered (TYC 1422-1328-1, magnitude in *STEREO*/HI-1A of 9.5, period 3.0999 days, $|e \times \cos \omega| = 0.175 \pm 0.025$ with primary and secondary eclipses both 0.1 mag deep and BD +09 485, magnitude in *STEREO*/HI-1A of 9.15, period 4.5293 days, $|e \times \cos \omega| = 0.125 \pm 0.025$ with primary eclipses 0.15 mag deep and secondary eclipses 0.1 mag deep), amongst numerous other short-period variables. Periods have been extracted for a variety of stars showing sinusoidal-like variations in their lightcurve and some stars showing changes in behaviour on a year-by-year basis have been observed (eg. V 471 Tau, SZ Psc). Additional findings will be reported in due course.

7 ACKNOWLEDGEMENTS

The Heliospheric Imager (HI) instrument was developed by a collaboration that included the Rutherford Appleton Laboratory and the University of Birmingham, both in the United Kingdom, and the Centre Spatial de Liège (CSL), Belgium, and the US Naval Research Laboratory (NRL), Washington DC, USA. The *STEREO*/SECCHI project is an international consortium of the Naval Research Laboratory (USA), Lockheed Martin Solar and Astrophysics Lab (USA), NASA Goddard Space Flight Center (USA), Rutherford Appleton Laboratory (UK), University of Birmingham (UK), Max-Planck-Institut für Sonnensystemforschung (Germany), Centre Spatial de Liège (Belgium), Institut d’Optique Théorique et Appliquée (France) and Institut d’Astrophysique Spatiale (France). This research has made use of the SIMBAD database, operated at CDS, Strasbourg, France. This research has made use of NASA’s Astrophysics Data System. This research has made use of the statistical analysis package R (R Development Core Team 2008). This research has made use of version 2.31 PERANSO light curve and period analysis software, maintained at CBA, Belgium Observatory <http://www.cbabelgium.com>. This research is funded by the Science and Technology Facilities Council (STFC). This research made use of an IDL program to carry out a Lomb-Scargle periodogram analysis from Armagh Observatory at <http://www.arm.ac.uk/~csj/idl/PRIMITIVE/scargle.pro>. K. T. Wraight acknowledges support from an STFC studentship. Many thanks to the referee for numerous thoughtful and constructive comments that have improved the quality of the paper.

APPENDIX A: ECCENTRIC ECLIPSING BINARIES

The measurably eccentric eclipsing binaries are shown in Figure B2, along with the lightcurve of HD 173770, which al-

though not included in the sample owing to an inability to uniquely determine its period due to the small number of eclipses observed, nevertheless appears to be an eccentric eclipsing binary. The $|e \times \cos \omega|$ measured for this star is 0.108 ± 0.012 and the lightcurve shown is a phase-folding on a period of 25.145 days. The values of $|e \times \cos \omega|$ measured for the other stars can be found in Table B1. The identities of the stars are as given in the table, however in the cases where nearby stars may have contaminated the signal or be the real source of eclipses it was often the case that the eclipses would feature in multiple lightcurves and the ones selected for analysis were those that were clearer and had deeper eclipses and the higher SDE. Where this occurred, the table gives the name of a star that may be contaminating the lightcurve or be the real source of eclipses.

APPENDIX B: TABLES AND FIGURES

The sample of 263 eclipsing binaries, with the various statistics that have been collected for each is given here. Where data is not available, for example because secondary eclipses were not visible or the spectral type has yet to be determined, the entry is given as NA. Right ascension and declination are given in degrees. Primary eclipse depth and weighted mean magnitude are both in units of magnitudes. Periods are in units of days. The Box-Least-Squares (BLS) signal detection efficiency (SDE), the peak power from a Lomb-Scargle periodogram analysis and the Stetson variability index are all arbitrary scalar units. The estimates of minimum eccentricity ($|e \times \cos \omega|$) and the estimated errors in those estimates are all scalar values. The spectral type given is for the closest star to the listed co-ordinates from SIMBAD, the identity of which is given in the next column. The alternative nearby star is the identity of a nearby star that might be the source of the eclipses, rather than the closest star (this frequently occurs due to the 70 arc-second per pixel resolution of STEREO/HI-1A, as well as being due to nearby bright eclipsing binaries). The Known EB is a binary flag set to 1 if either star is recorded as showing eclipses and 0 otherwise.

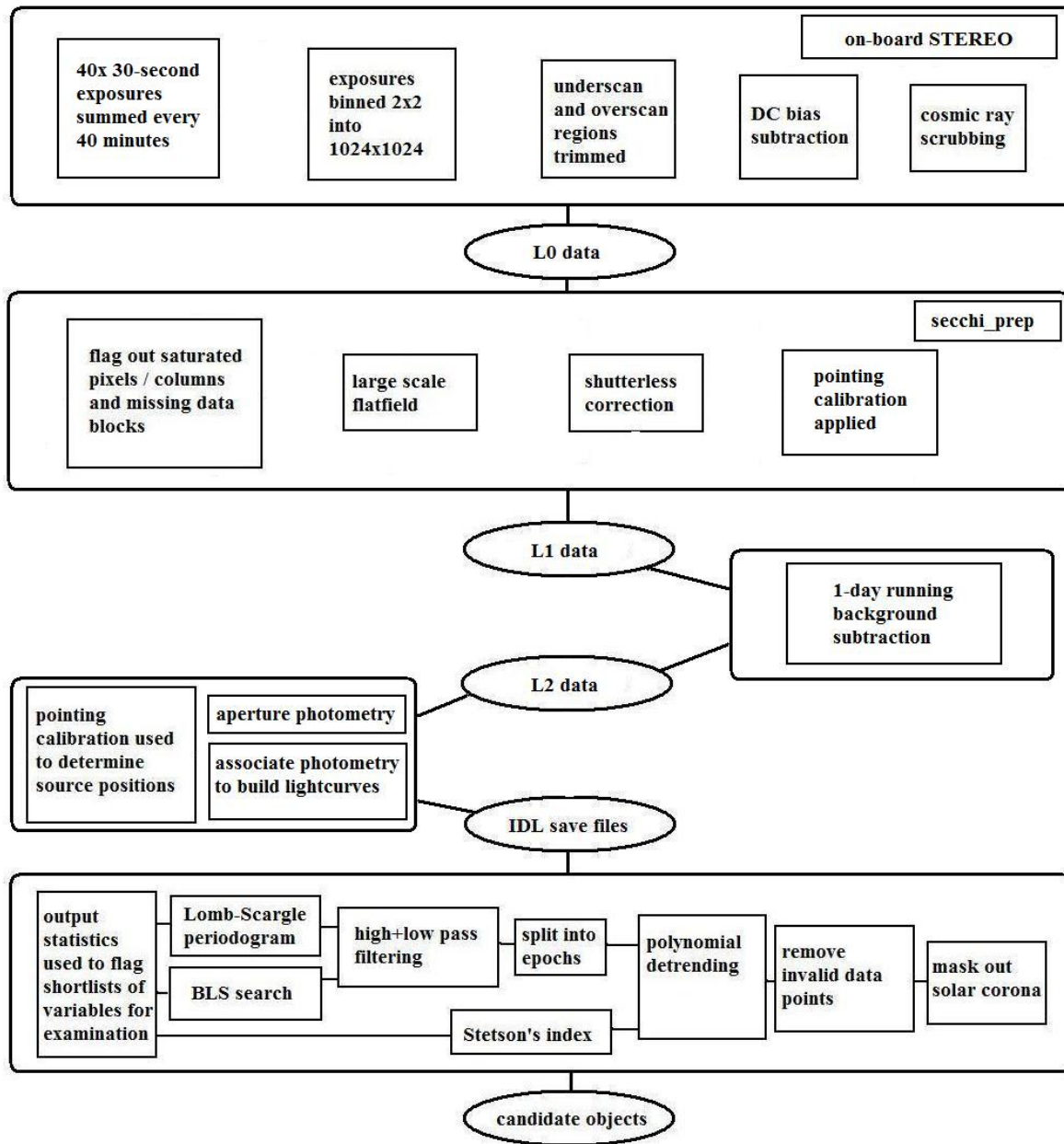


Figure B1. The *STEREO*/HI-1A data analysis pipeline.

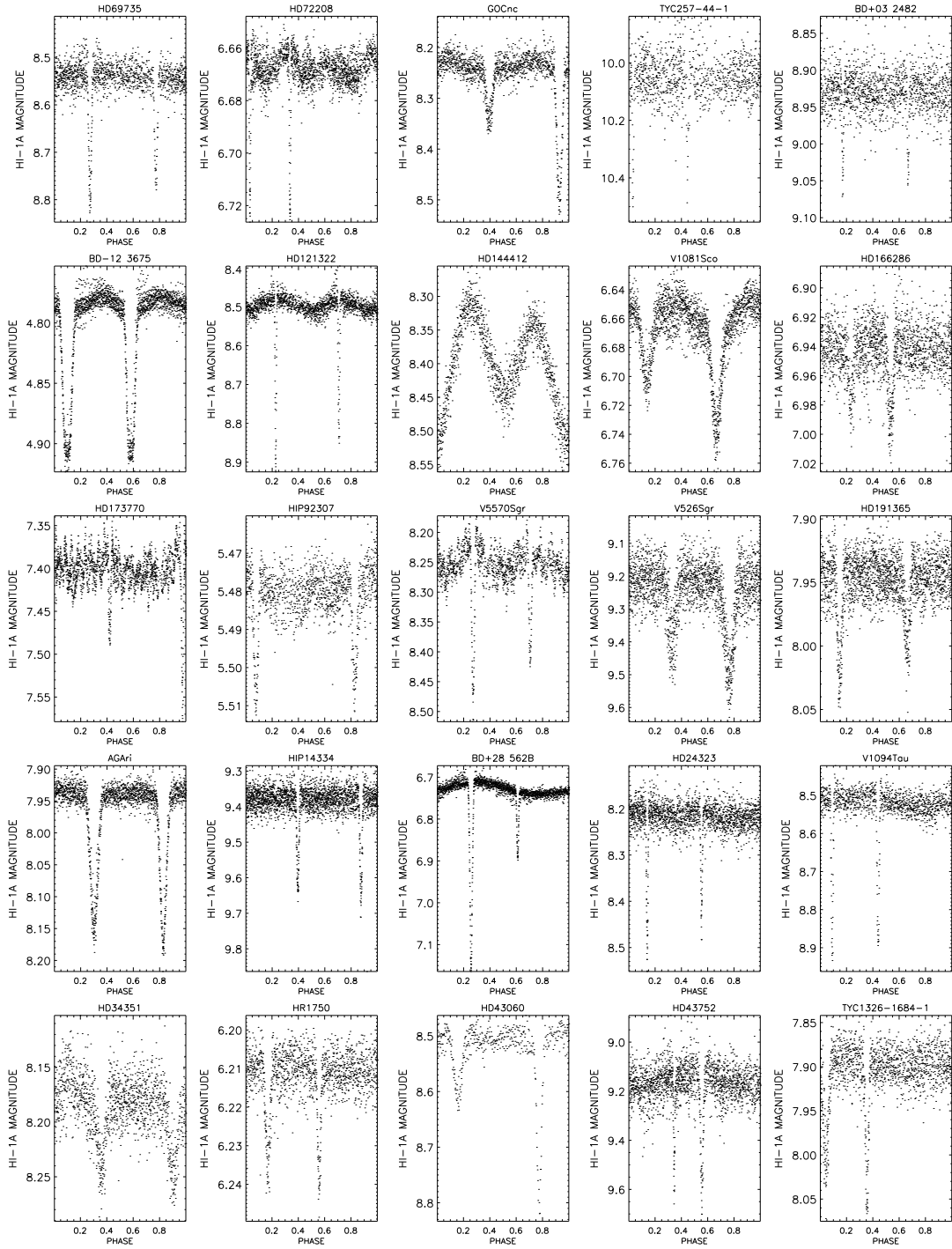


Figure B2. Lightcurves of all measurably eccentric EBs in the sample and the best-fitting lightcurve of HD 173770 (see Section 4).

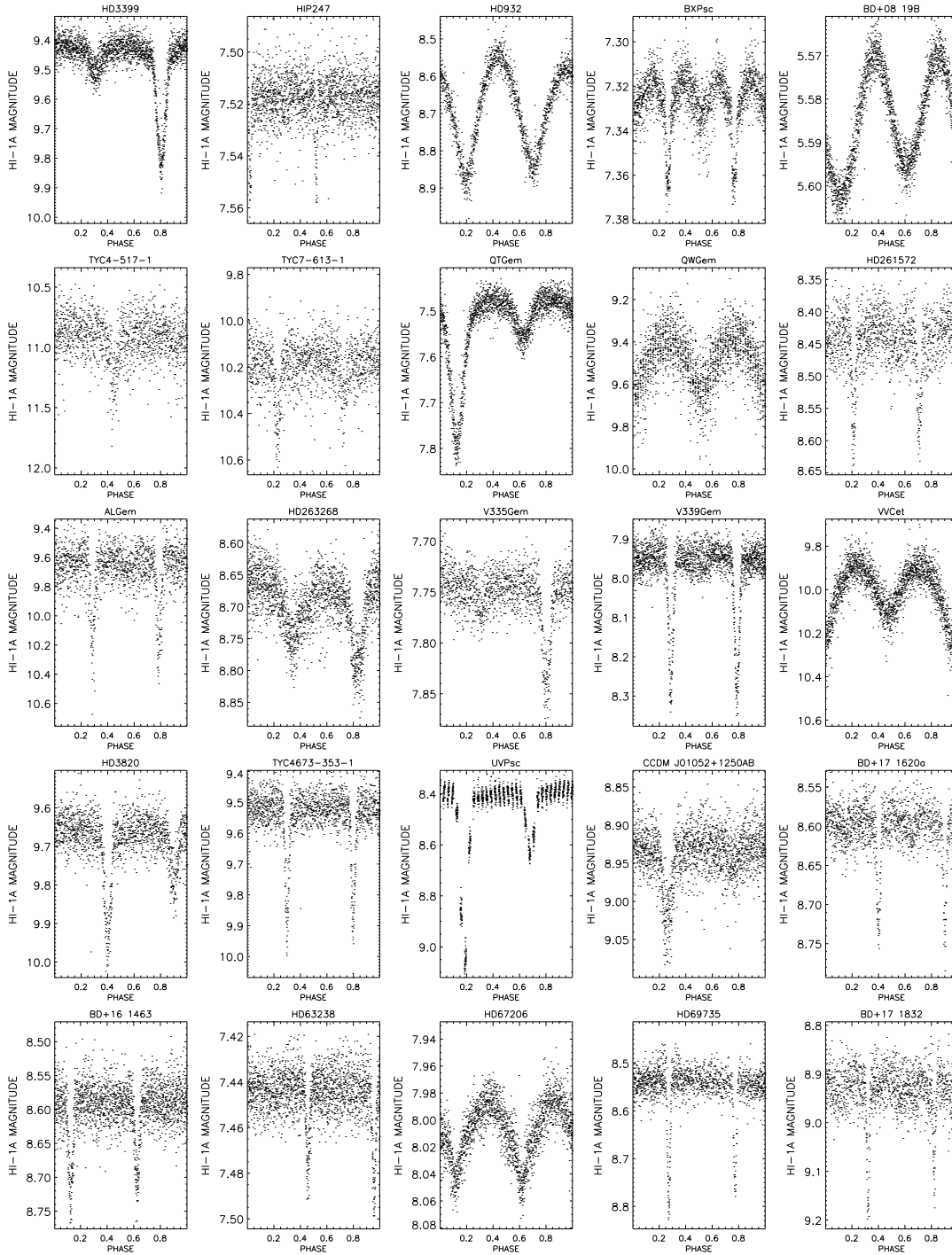


Figure B3. Lightcurves of all EBs in the sample including HD 173770 (see Section 4). For Supporting Information only.

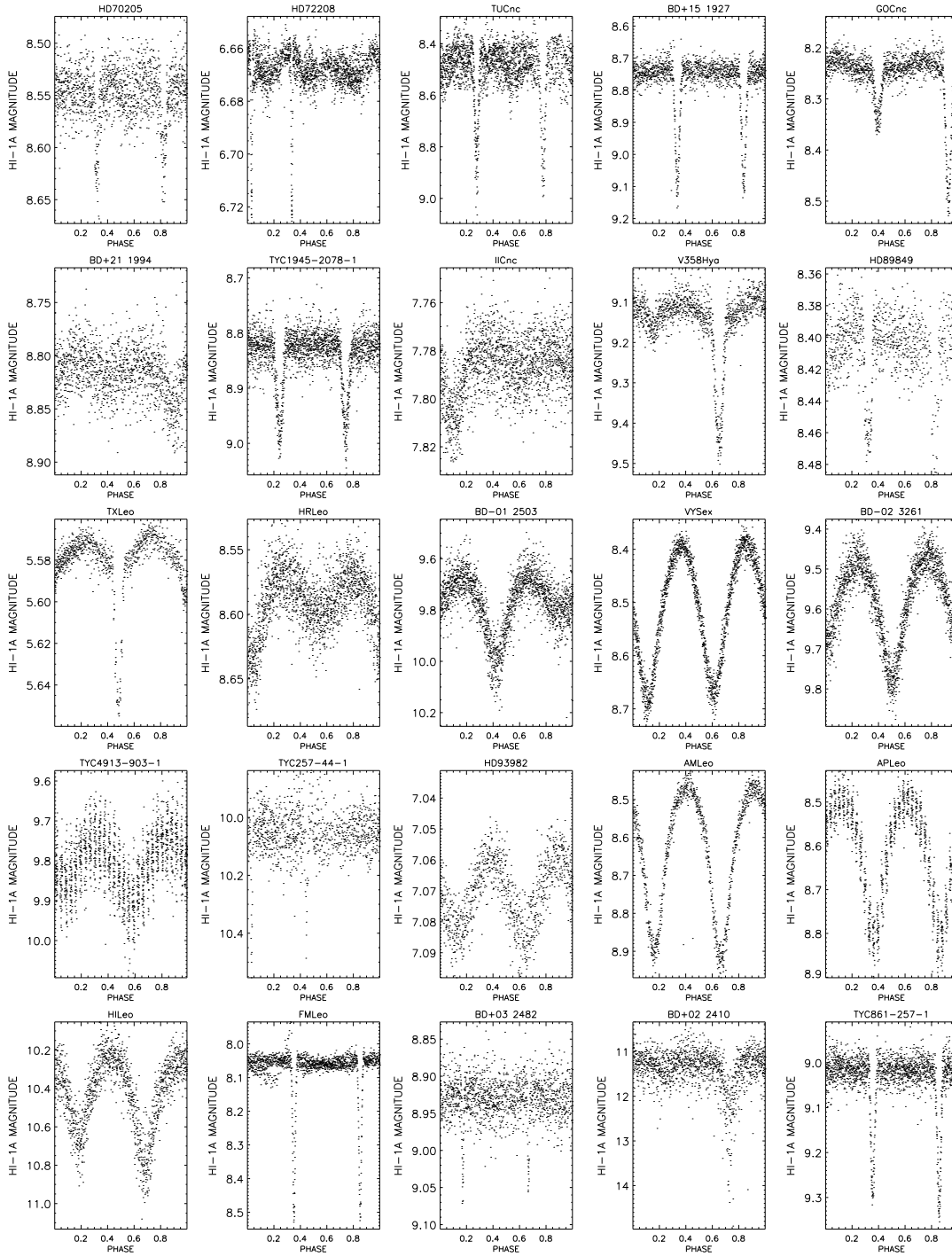


Figure B4. Lightcurves of all EBs in the sample including HD 173770 (see Section 4). For Supporting Information only.

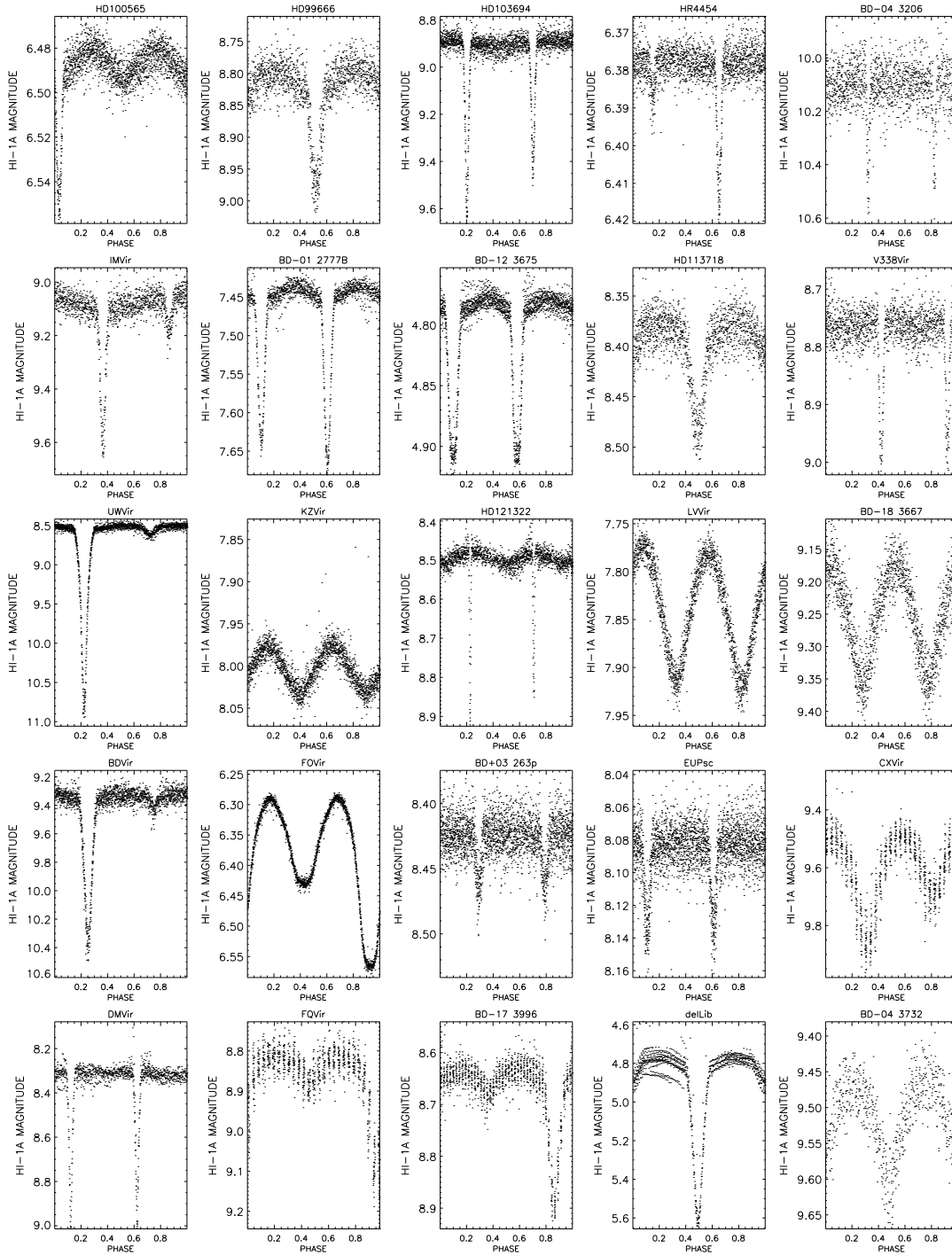


Figure B5. Lightcurves of all EBs in the sample including HD 173770 (see Section 4). For Supporting Information only.

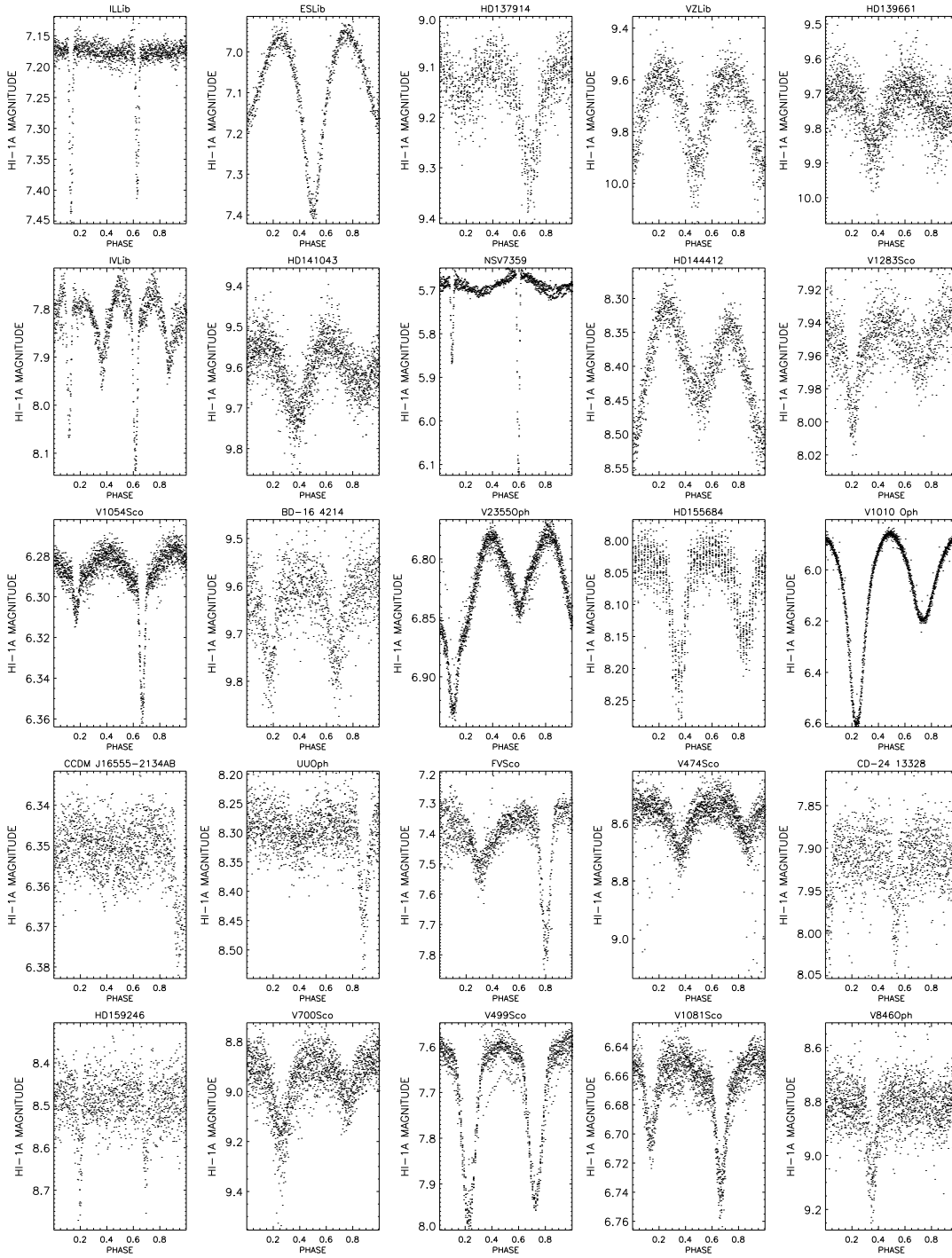


Figure B6. Lightcurves of all EBs in the sample including HD 173770 (see Section 4). For Supporting Information only.

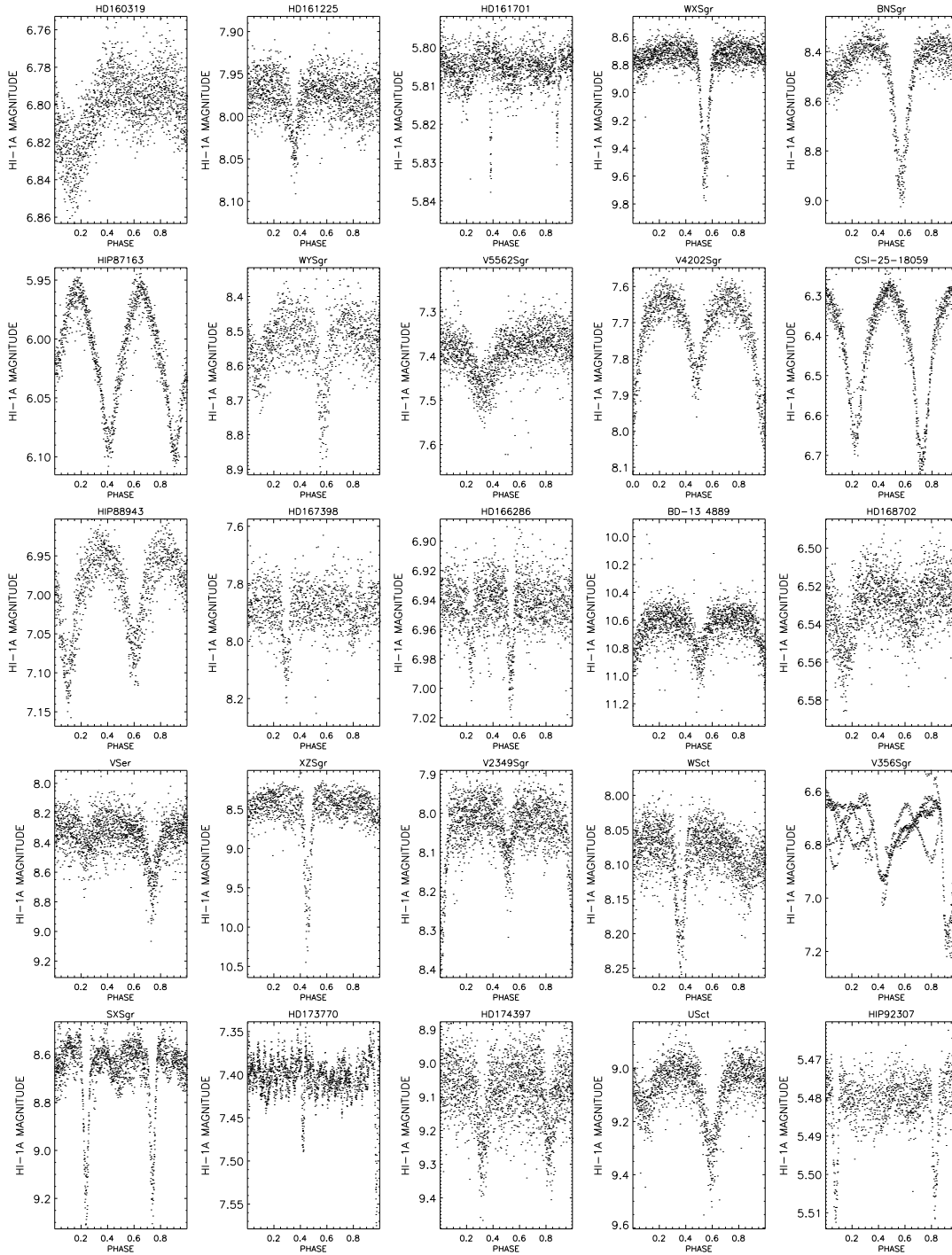


Figure B7. Lightcurves of all EBs in the sample including HD 173770 (see Section 4). For Supporting Information only.

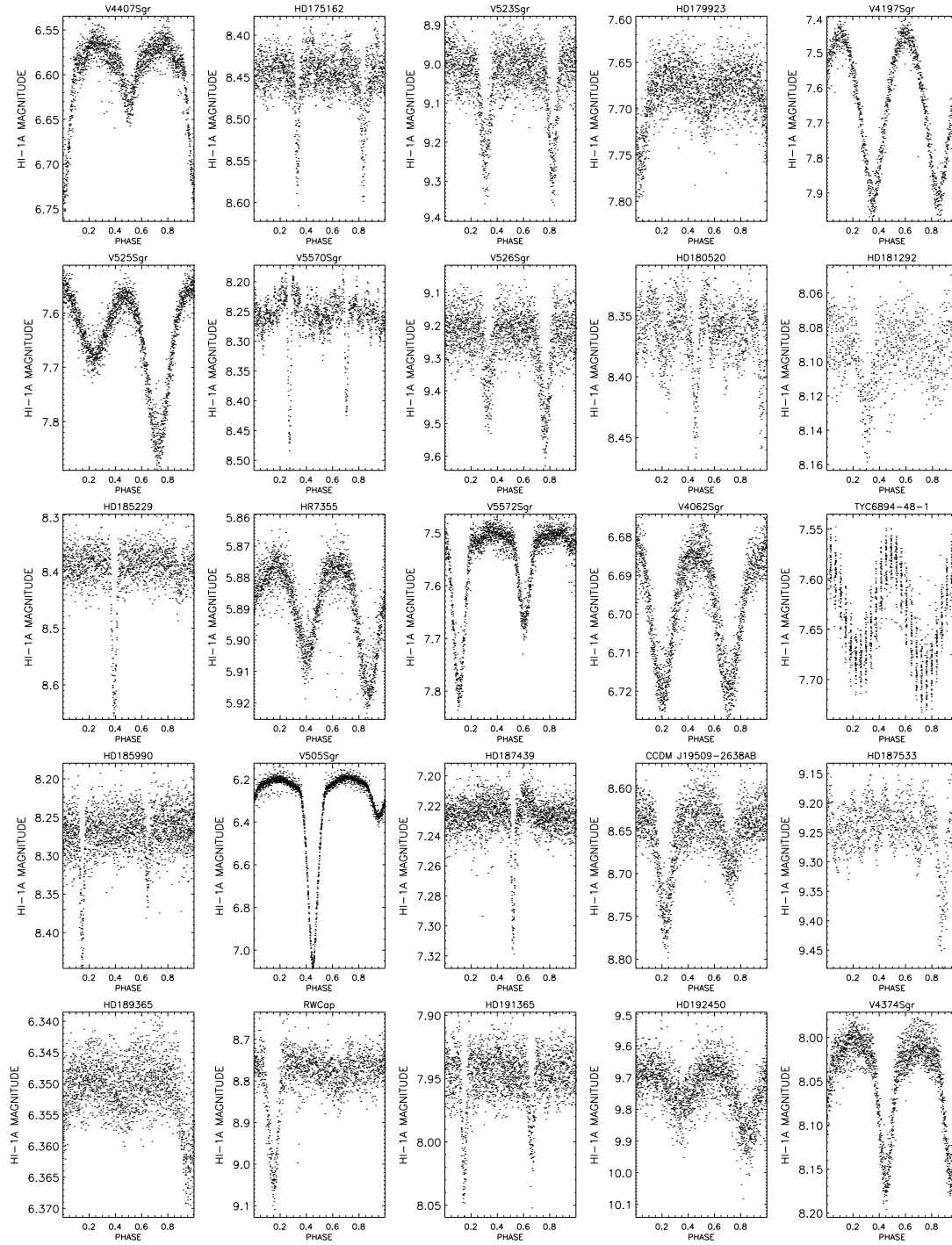


Figure B8. Lightcurves of all EBs in the sample including HD 173770 (see Section 4). For Supporting Information only.

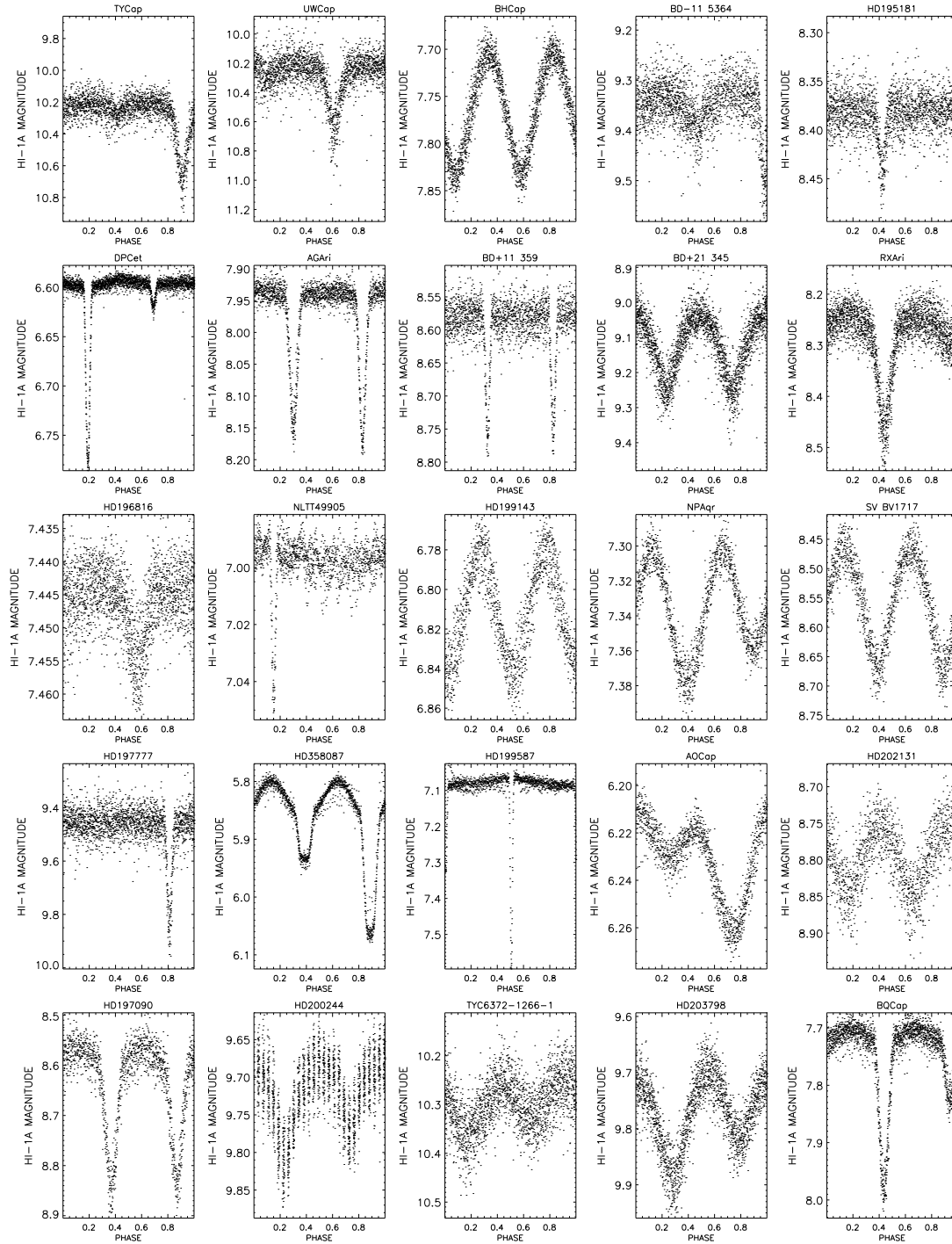


Figure B9. Lightcurves of all EBs in the sample including HD 173770 (see Section 4). For Supporting Information only.

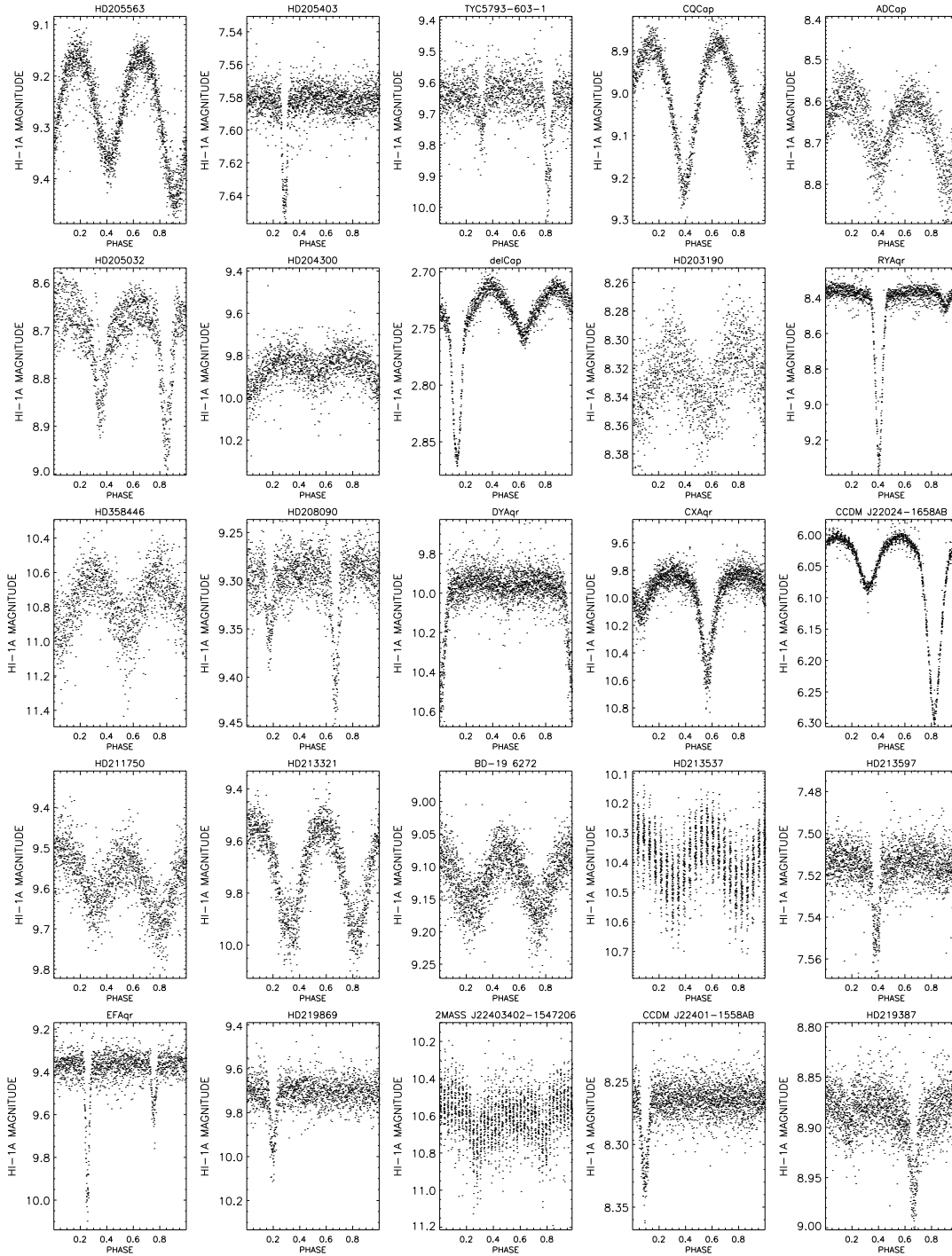


Figure B10. Lightcurves of all EBs in the sample including HD 173770 (see Section 4). For Supporting Information only.

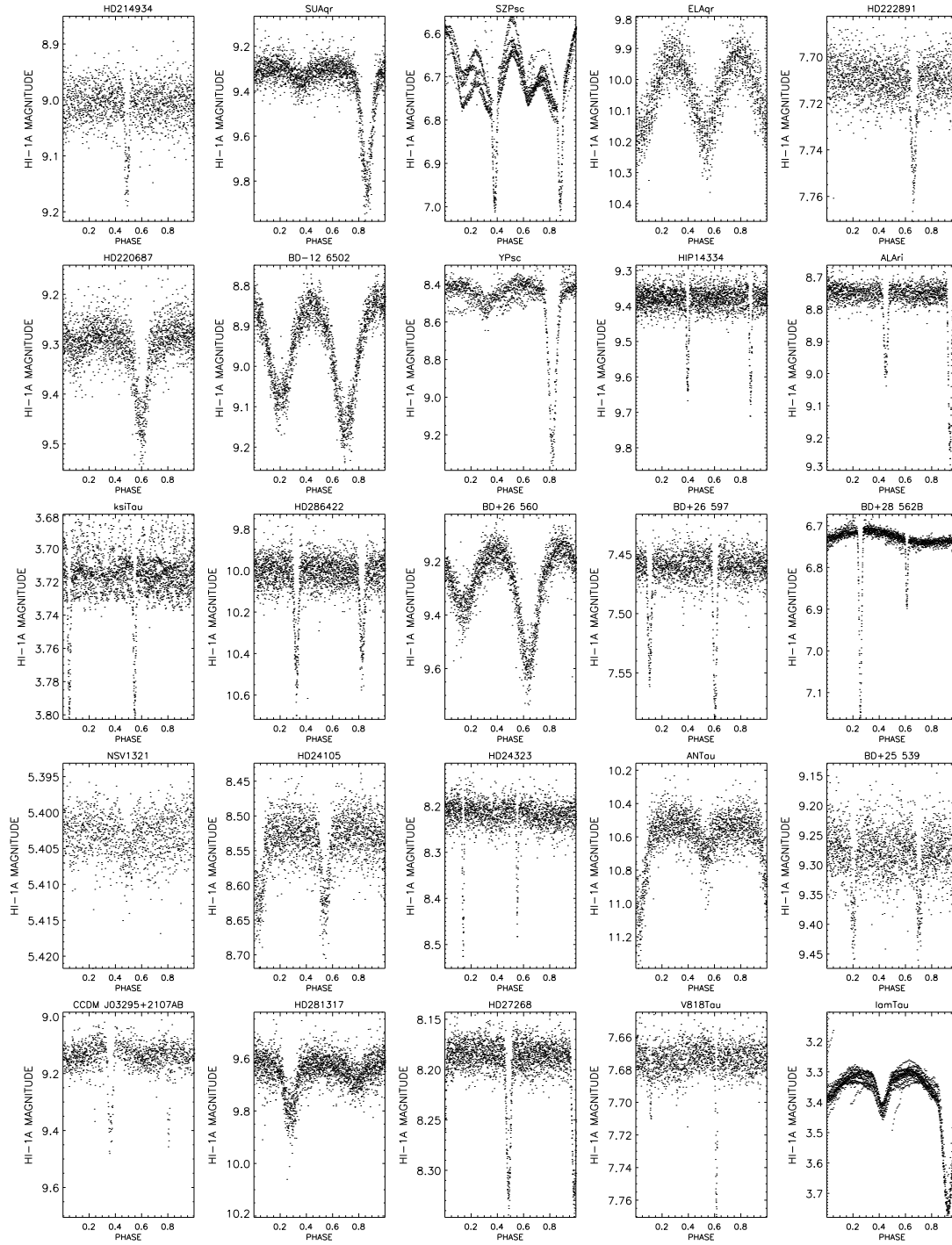


Figure B11. Lightcurves of all EBs in the sample including HD 173770 (see Section 4). For Supporting Information only.

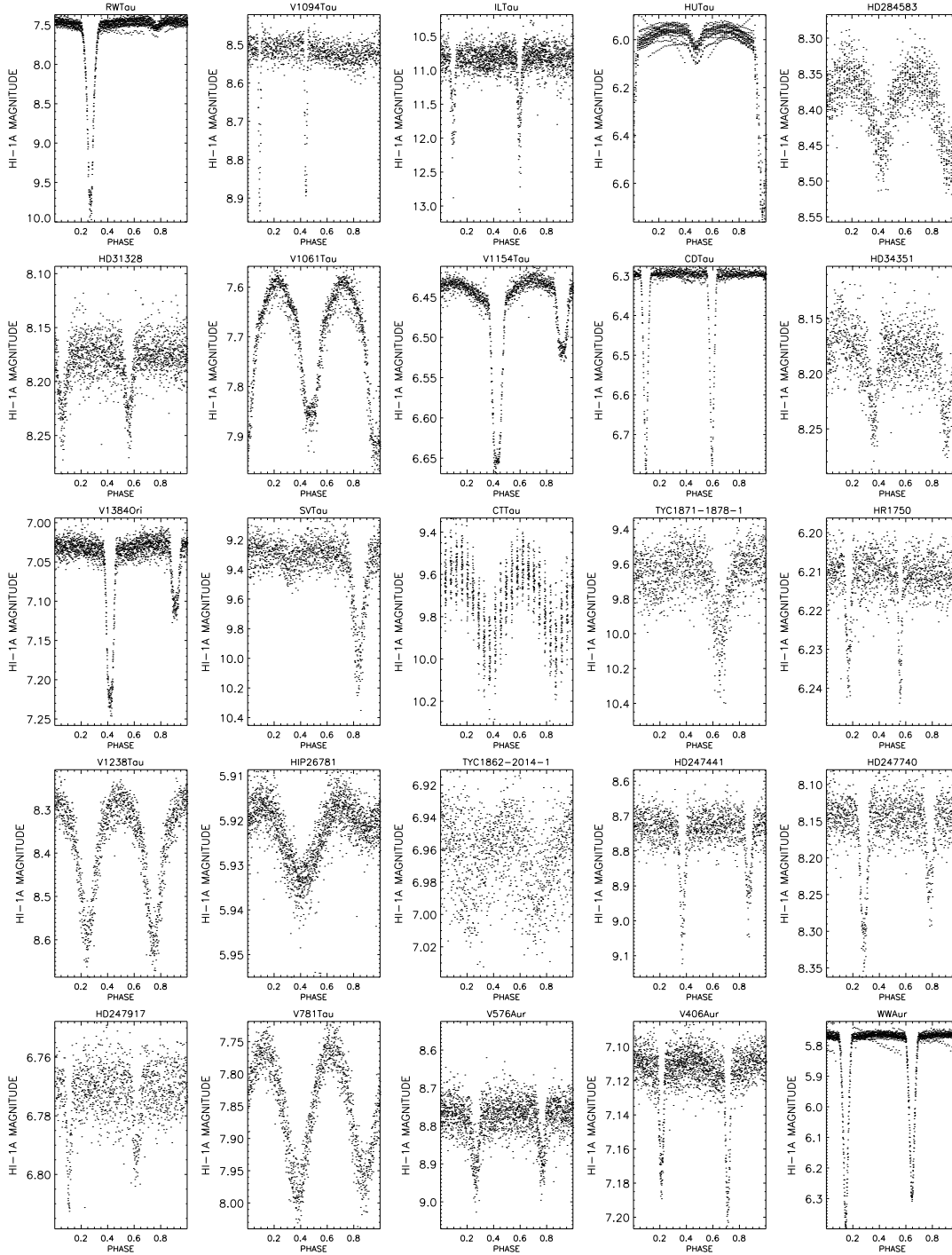


Figure B12. Lightcurves of all EBs in the sample including HD 173770 (see Section 4). For Supporting Information only.

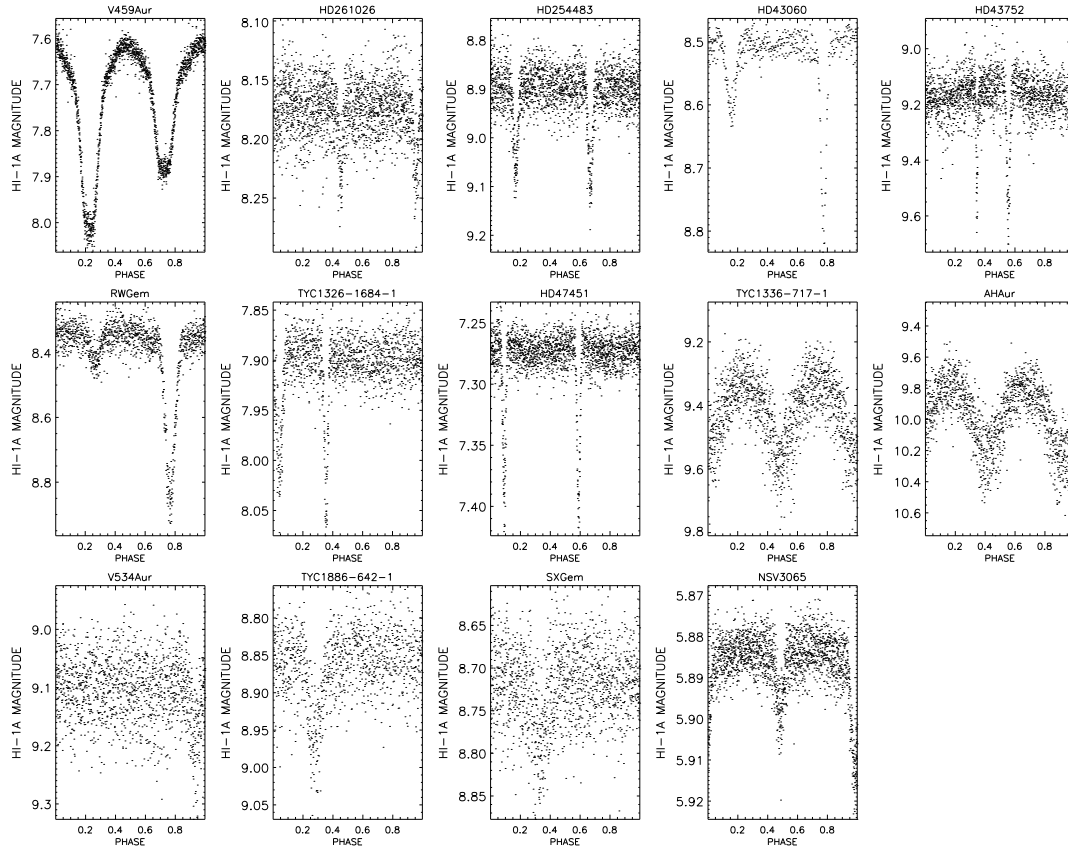


Figure B13. Lightcurves of all EBs in the sample including HD 173770 (see Section 4). For Supporting Information only.

Table B1: 263 eclipsing binaries found from *STEREO*/HI-1A data.

RA	DEC	Primary eclipse depth	Period	Weighted mean magnitude	BLS SDE	Stetson index	Peak Lomb-Scargle power	$ e \times \cos \omega $	\pm error in $ e \times \cos \omega $	Spectral type	Identity	Alternative nearby star	Known EB
58.306	30.1915	0.15	0.79165	9.6355	4.985	0.089959	163.27	0.014	0.05	A0	HD281317	NA	0
99.8127	31.5917	0.06	4.763	8.1252	4.0087	0.095906	83.309	NA	NA	F5	HD261026	AKAur	1
92.5473	30.0289	0.15	0.9815	8.7237	4.9764	0.10818	111.68	0.002	0.02	A0	V576Aur	NA	1
94.4646	32.5046	0.07	2.7361	7.0957	5.7669	0.12152	102.39	0.008	0.024	A3	V406Aur	NA	1
98.1133	32.4549	0.55	2.5250	5.7419	6.1559	95.241	101.2	0.03	0.04	A3m	WWAur	NA	1
98.9069	32.5768	0.4	1.065	7.7216	4.163	4.0988	272.15	0.00	0.036	B8	V459Aur	NA	1
101.605	31.4128	0.13	4.6835	8.6636	3.1958	0.10923	189.26	0.025	0.07	G5	HD263268	HD263212	0
33.8366	22.5697	0.2	1.02775	8.3924	5.9916	1.1283	133.77	0.01	0.03	F2V	RXAri	NA	1
37.7781	22.1983	0.25	0.3963	9.1747	3.7634	0.1098	294.49	0.00	0.06	F8	BD +21 345	NA	0
50.8846	25.8994	0.1	1.30555	9.2946	8.3623	0.034856	81.708	NA	NA	F5	BD +25 539	NA	0
52.3671	21.1134	0.2	4.98975	9.1	4.5718	0.1323	40.661	NA	NA	F2	CCDM J03295 +2107AB	NA	0
52.2775	27.4136	0.4	1.0	9.2641	4.1739	0.59102	268.03	0.01	0.036	F2	BD +26 560	NA	1
55.0698	26.8486	0.12	6.114	7.4839	6.2441	0.075213	53.906	0.00	0.02	B9	BD +26 597	NA	0
55.1605	28.7716	0.45	8.1665	6.7556	7.38	3.8155	34.838	0.294	0.006	A2V	BD +28 562B	HD22766	1
57.0867	23.4213	0.01	2.2663	5.3929	2.764	0.0013492	227.86	NA	NA	B8V	NSV1321	NA	0
57.8397	25.6354	0.15	0.63145	8.4441	4.8421	0.073541	138.34	NA	NA	G5	HD24105	NA	0
58.2809	25.5354	0.3	6.53065	8.2552	4.8853	0.21381	35.026	0.18	0.006	A0	HD24323	SXTau	1
59.0473	29.523	0.7	1.6144	10.2486	6.14114	0.25888	172.29	0.01	0.06	A3	ANTau	NA	1
69.5660	20.6847	0.75	2.0555	5.8251	7.189	100.44	69.73	0.01	0.03	B8V	HUTau	NA	1
60.9763	28.126	2.3	2.7778	7.9245	6.5421	35.085	73.255	0.00	0.035	B8Ve	RWTau	NA	1
61.8078	29.309	1.2	5.3604	10.9617	6.4905	0.327	63.897	NA	NA	NA	ILTau	NA	1
63.015	21.9474	0.4	9.0	8.5775	4.4708	0.21727	25.498	0.305	0.02	G0	V1094Tau	NA	1
69.7778	22.7121	0.1	0.7641	8.3943	4.2479	0.05307	166.57	NA	NA	B5	HD284583	NA	0
73.9828	27.8354	0.06	1.2222	8.1691	4.9429	0.022643	109.84	0.005	0.04	F8	HD31328	AQTau	1
74.7198	24.4957	0.38	0.6944	7.6702	4.8047	24.254	199.61	NA	NA	B5	V1061Tau	NA	1
76.4072	23.0611	0.23	1.7778	6.5015	4.9423	1.9962	96.445	0.02	0.02	B5	V1154Tau	NA	1
79.3798	20.1318	0.5	1.71755	6.3583	6.5897	13.857	51.274	NA	NA	F7V	CDTau	NA	1
79.4109	20.5354	0.07	2.6419	8.2016	3.5365	0.015735	120.34	0.095	0.04	B9	HD34351	NA	0
80.2472	27.9573	0.03	3.315	6.2125	5.0512	0.0094084	42.977	0.225	0.01	B9IV	HR1750	NA	0

85.3374	29.4874	0.02	0.674	5.9259	3.4628	0.044185	143.2	0.035	0.06	B8IV	HIP26781	HD37647	0
85.5607	22.3714	0.3	1.1218	8.3929	3.2723	0.62529	187.94	NA	NA	A0	V1238Tau	NA	1
85.8421	24.1209	0.06	2.0045	6.9761	3.1702	0.05839	163.67	NA	NA	A	TYC 1862 2014 1	HD37979	0
87.0687	20.7695	0.28	2.43055	8.6347	4.841	0.23099	68.82	0.005	0.04	NA	HD247740	HD38693	0
86.764	28.226	0.25	4.2676	8.7384	4.80195	0.1336	51.331	0.00	0.02	A0	HD247441	NA	0
87.3169	24.2109	0.035	2.6897	6.7581	3.9495	0.0052434	62.349	0.011	0.03	A3	HD247917	HD38808	0
87.5547	26.962	0.2	0.34508	7.8473	3.7413	0.25811	212.95	0.005	0.03	G0	V781Tau	NA	1
88.0221	28.0927	0.75	2.16665	9.35634	6.1146	0.81875	75.385	0.025	0.100	B9	SVTau	NA	1
89.8347	28.0275	0.5	1.3496	9.7615	3.8609	0.11148	83.227	NA	NA	NA	TYC 1871 1878 1	NA	0
89.7362	27.0541	0.45	0.66685	9.53182	4.096	0.18057	214.68	0.01	0.08	B5	CTTau	NA	1
93.4814	21.3804	0.2	3.1505	7.9754	5.5903	0.13942	64.155	0.365	0.03	NA	TYC 1326 1684 1	FTOri	1
90.3669	23.141	0.5	2.8655	8.5366	5.4542	1.2502	72.193	0.00	0.05	B6V	RWGem	NA	1
94.8144	28.4398	0.45	10.8922	9.1588	3.4064	0.24165	61.223	0.575	0.005	A2	HD43752	NA	1
95.0105	26.3303	0.1	2.7483	8.794	4.413	0.02671	41.01	NA	NA	NA	TYC 1886 642 1	NA	1
96.0032	20.4702	0.33	0.351	9.3721	3.5966	0.060442	172.6	NA	NA	NA	TYC 1336 717 1	NA	0
96.5206	27.999	0.5	0.4934	10.025	3.4552	0.22515	183.59	NA	NA	G1	AHAur	NA	1
96.5995	27.9456	0.1	2.1419	9.1058	3.9544	0.020826	38.65	NA	NA	NA	V534Aur	NA	1
97.0887	20.5330	0.08	1.3668	8.6545	3.487	0.0321	33.79	NA	NA	A0	SXGem	NA	1
99.888	28.2632	0.03	1.8797	5.8952	5.0919	0.050436	112.29	0.005	0.04	B7III	NSV3065	NA	0
100.122	22.8955	0.15	2.04755	8.401	4.387	0.08155	77.07	0.01	0.02	G0	HD261572	NA	0
102.692	29.4531	0.3	0.3581	9.5661	3.787	0.34595	206.45	NA	NA	G0	QWGem	NA	1
104.411	20.8924	0.7	1.3913	9.6675	4.403	0.145	44.64	NA	NA	F6V	ALGem	NA	1
105.523	21.7981	0.09	1.7678	7.7499	5.9235	0.0376	70.74	0.005	0.04	B9	V335Gem	NA	1
109.714	29.1009	0.33	2.88035	8.3468	6.5489	2.2977	93.296	NA	NA	F2	V339Gem	NA	1
117.254	28.574	0.045	1.425	7.4336	5.884	0.02342	54.56	0.01	0.02	F0	HD63238	STF 1144AB	0
125.384	21.5953	0.06	1.6054	8.5395	5.9816	0.006909	58.784	NA	NA	A5	HD70205	NA	0
131.067	25.0757	0.16	1.19035	8.8014	5.6777	0.06538	109.62	NA	NA	NA	TYC 1945 2078 1	TYC 1945 1438 1	0
133.458	26.9132	0.025	0.5342	7.8157	4.072	0.05791	95.53	0.015	0.200	G8V	IICnc	NA	0
138.547	20.7034	0.05	0.6855	8.837	3.428	0.0020536	105.924	NA	NA	G5	BD +21 1994	BD +21 1994p	0
16.3016	12.8321	0.11	1.62785	8.933	5.922	0.01696	114.13	0.015	0.05	G0	CCDM J01052 +1250AB	BD +12 131C	0
26.2229	19.8568	0.05	0.8463	8.0935	6.019	0.01728	106.64	NA	NA	F0	EUPsc	NA	1

39.128	12.1424	0.20	1.80245	8.6189	6.2292	0.059477	52.623	NA	NA	F8	BD +11 359	NA	1
36.6123	12.8988	0.25	1.9631	7.9653	5.3368	0.32205	98.264	0.055	0.015	B9	AGAri	NA	1
40.6514	12.7355	0.45	3.7474	8.7802	6.514	0.2791	36.44	0.02	0.02	F8	ALAri	NA	1
59.8049	12.6382	0.45	2.32225	10.115	5.8665	0.15452	68.537	NA	NA	A2	HD286422	NA	0
60.1701	12.4903	0.4	3.9529	3.4625	5.8633	1374.4	140.8	0.005	0.02	B3V	lamTau	NA	1
64.7172	12.9248	0.13	2.06345	8.1948	6.2857	0.07836	72.31	NA	NA	A0	HD27268	NA	0
64.4123	16.9479	0.08	5.6093	7.6616	5.5192	0.01604	41.01	0.005	0.01	G8V	V818Tau	NA	1
89.2108	16.3551	0.19	3.7802	7.0654	5.9208	0.816	97.582	0.015	0.02	B2V	V1384Ori	NA	1
94.2841	14.4566	0.20	1.51305	8.9091	5.7367	0.16955	68.938	NA	NA	F8IV	HD254483	GSC 00743 01238	0
93.6901	13.2113	0.30	2.73	8.5239	6.3801	0.047377	42.956	0.23	0.02	B3V	HD43060	NA	0
99.8207	13.6861	0.13	4.55025	7.2869	7.6666	0.22473	46.076	NA	NA	K0	HD47451	NA	0
102.069	14.5924	0.30	1.6199	7.4618	5.1785	2.5358	164.603	0.015	0.04	A0	QTGem	NA	1
110.796	15.9870	0.12	1.69445	8.6423	7.2193	0.072526	71.826	NA	NA	A7V	BD +16 1463	NA	0
114.053	16.9029	0.15	2.80005	8.5922	5.9309	0.028149	59.059	NA	NA	K2	BD +17 1620a	TXGem	1
121.8	10.147	0.07	1.8852	7.9903	5.1821	0.089832	276.58	0.015	0.04	F0	HD67206	NA	0
124.75	19.976	0.25	5.3899	8.5718	6.4434	0.11706	35.476	0.014	0.01	A3	HD69735	NA	0
125.993	17.1141	0.25	3.5792	8.9663	5.8786	0.054716	54.377	NA	NA	A2	BD +17 1832	NA	0
133.232	14.8165	0.35	1.8554	8.7986	6.7368	0.29514	48.61	NA	NA	A0	BD +15 1927	Cl* NGC 2632 KP 102662	0
139.409	16.705	0.27	3.65	8.2735	5.3567	0.19792	69.855	0.08	0.03	A0	GOCnc	NA	1
168.984	14.7035	0.3	4.4507	9.0733	5.7337	0.1575	52.187	0.00	0.015	NA	TYC 861 257 1	NA	0
173.541	11.0239	0.032	2.2096	6.3907	6.3079	0.11581	61.79	0.009	0.02	A2m	HR4454	NA	0
0.765435	8.26129	0.03	2.2604	7.4773	5.387	0.010015	57.588	NA	NA	F0	HIP 247	HIP 248	0
1.36379	4.80649	0.4	2.1027	10.994	3.267	0.0691	61.1486	NA	NA	NA	TYC 4 517 1	NA	0
3.43064	6.9384	0.3	0.951	8.701	3.789	0.398	223.12	0.015	0.03	A5	HD932	NA	0
4.47026	7.86604	0.04	3.86045	7.3076	4.012	0.01586	206.115	NA	NA	A5	BXPsc	NA	1
3.74693	8.81828	0.032	0.8417	5.565	2.976	0.0978	314.956	0.015	0.03	A7	BD +08 19B	UUPsc	1
2.19967	5.47131	0.3	2.3999	10.246	3.619	0.2143	59.166	0.015	0.03	NA	TYC 7 613 1	NA	0
19.2297	6.8117	0.7	0.8611	8.4686	6.1005	1.0814	100.71	0.015	0.02	G5	UVPsc	NA	1
28.7275	3.78465	0.05	1.2959	8.4435	5.5528	0.0033295	63.903	NA	NA	NA	BD +03 263p	BD +03 263s	0

32.464	3.76935	0.18	2.3682	6.6093	8.0387	0.61444	57.542	0.005	0.015	A2	DPCet	NA	1
46.2098	8.11422	0.29	5.9971	9.3981	6.365	0.050353	41.737	0.13	0.01	F8	HIP 14334	NA	0
51.7923	9.73267	0.07	3.5732	3.7049	7.3388	10.227	38.366	NA	NA	B9Vn	ksiTau	NA	1
127.977	9.81409	0.06	22.013	6.6731	4.5847	0.083666	44.264	0.391	0.006	B9p	HD72208	NA	0
133.069	9.08854	0.4	5.5615	9.1992	3.5363	9.2918	64.636	NA	NA	A2	TUCnc	NA	1
143.758	4.75613	0.3	3.0095	9.009	6.2857	286470	106.75	0.005	0.04	A2	V358Hya	NA	1
155.541	6.21829	0.08	3.07835	8.3795	3.1369	0.0061672	42.305	NA	NA	F8	HD89849	AG +06 1309	0
158.759	8.65043	0.07	2.445	5.5845	5.2227	0.14123	65.099	0.025	0.03	A2V	TXLeo	NA	1
162.333	2.57512	0.5	8.0319	10.053	6.7082	0.017853	32.705	0.183	0.01	NA	TYC 257 44 1	NA	0
162.738	3.59068	0.03	0.4325	7.0637	4.025	0.002475	125.72	NA	NA	A2	HD93982	NA	0
165.545	9.89519	0.42	0.3658	8.6466	3.935	0.4847	145.74	NA	NA	F8Vn	AMLeo	NA	1
166.271	5.15179	0.32	0.4306	8.5874	3.2822	0.37463	161.93	0.00	0.04	F8V	APLeo	NA	1
168.070	1.31822	0.55	0.3116	10.391	3.703	0.0869	183.6	0.00	0.06	NA	HILeo	NA	1
168.188	0.348007	0.47	6.7287	8.0948	7.2493	1.02896	28.736	0.004	0.006	F8	FMLeo	NA	1
169.662	2.82139	0.1	9.1784	8.959	5.097	0.0075	26.6756	0.015	0.01	G0	BD +03 2482	BD +03 2483A	0
169.789	1.95757	1.1	1.29785	11.543	5.225	0.211	81.82	NA	NA	F8	BD +02 2410	NA	0
179.134	7.29747	0.75	2.2392	8.937	5.7896	0.81757	59.004	0.005	0.006	K2	HD103694	NA	0
198.095	2.65383	0.06	1.1318	8.0144	4.2689	0.17505	296.99	0.00	0.06	F2	KZVir	NA	1
202.446	1.09535	0.27	0.7756	6.3652	4.5741	12.042	273.66	0.015	0.05	A2	FOVir	CCDM J13298 +0106AB	1
338.136	1.58245	0.025	2.4238	7.493	6.3662	0.29712	79.855	NA	NA	F0	HD213597	HD213598	0
348.349	2.67544	0.27	3.96565	6.733	6.4122	7.8083	162.97	NA	NA	K1 IV- V	SZPsc	NA	1
353.606	7.9246	0.9	3.7657	8.636	5.285	4.542	65.128	NA	NA	A3V	YPsc	NA	1
9.2297	-	0.35	3.4885	9.4566	6.3841	0.23564	138.12	0.005	0.08	A5	HD3399	NA	1
13.9303	5.87404	0.4	0.5224	10.036	3.9492	0.18227	255.32	0.025	0.05	A5	VVCet	NA	1
10.2136	2.09399	0.3	1.6405	9.7072	5.9898	0.038305	93.877	0.005	0.03	F8	HD3820	FASTT28	0
11.5631	-	0.45	1.6900	9.6328	7.2307	0.093337	59.875	NA	NA	NA	TYC 4673 353 1	SDSS J004617.88 -000130.3	0
160.922	0.0386658	0.15	0.77895	9.9023	3.3872	0.039807	160.96	0.035	0.08	NA	TYC 4913 903 1	NA	0
162.624	-	0.3	0.4434	8.5033	3.3536	0.50124	268.8	0.015	0.02	F9.5V	VYSex	NA	1

164.775	-	0.3	1.0713	9.5849	4.3149	0.17634	261.69	0.005	0.05	NA	BD -02	NA	0
	3.54405										3261		
166.176	-	0.075	1.0847	8.591	4.6747	0.010763	207.77	0.025	0.140	F2	HRLeo	NA	1
	2.97221												
169.152	-	0.3	0.6288	9.8227	4.279	0.15639	218.56	0.015	0.07	NA	BD -01	NA	0
	1.90306										2503		
171.997	-	0.18	1.0143	8.8186	6.0283	0.04405	83.213	0.005	0.100	F2	HD99666	BD -01	0
	1.92144											2527B	
173.589	-5.5271	0.06	2.5670	6.5105	7.6481	0.06868	140.77	NA	NA	A2	HD100565	NA	0
181.587	-	0.4	2.7113	10.121	6.0989	0.036731	31.688	NA	NA	NA	BD -04	NA	0
	4.91402										3206		
192.411	-	0.5	1.3086	9.1087	6.6385	0.23859	55.119	0.015	0.024	G5	IMVir	NA	1
	6.07913												
197.118	-	0.2	2.7323	7.4267	6.0494	0.57602	93.207	0.001	0.009	F8	BD -01	HYVir	1
	2.68878										2777B		
208.716	-	0.42	6.6950	8.4903	6.0823	0.31388	24.374	0.045	0.01	F8	HD121322	NA	0
	2.38036												
220.288	-	0.18	0.3846	9.4452	2.8371	0.0097679	66.192	0.015	0.150	F8	BD -04	NA	0
	5.09566										3732		
225.243	-	0.85	2.3273	4.9170	6.3210	536.33	70.608	0.005	0.10	B9.5V	delLib	NA	1
	8.51894												
323.766	-3.7349	0.06	2.4449	7.5587	6.7961	0.053739	48.11	NA	NA	F5	HD205403	NA	0
328.78	-	0.25	1.8636	9.6842	5.7501	0.053637	51.422	0.007	0.02	K0V	TYC 5793	NA	0
	9.79926										603 1		
334.768	-	0.5	2.1597	9.9316	6.7132	0.31543	90.597	0.04	0.12	A0	DYAqr	NA	1
	2.64167												
338.933	-	0.7	0.556	10.003	4.5452	1.5886	210.04	0.015	0.05	F2pv	CXAqr	FASTT1583	1
	0.692436												
345.33	-6.4376	0.6	2.8536	9.4475	5.8903	5.8698	44.337	0.01	0.02	G0	EFAqr	NA	1
349.842	-	0.25	3.03095	9.8713	5.5423	0.03644	55.451	NA	NA	F8	HD219869	G273 -14	0
	8.87043												
356.826	-	0.28	0.4814	9.8908	4.3021	0.072444	248.93	0.015	0.07	F	ELAqr	NA	1
	8.08669												
356.162	-	0.04	1.59495	7.7152	6.0264	0.0062216	57.745	NA	NA	F8	HD222891	2MASS	0
	8.84879											J23443838	
190.304	-	0.13	3.14445	4.8099	5.0159	15.226	148.89	0.04	0.03	NA	BD-12	VVCrv	1
	13.0246										3675		
196.428	-12.37	0.1	1.581	8.3555	4.8238	0.025355	97.58	0.005	0.04	F8	HD113718	NA	0
197.823	-	0.22	2.99275	8.789	6.398	0.074939	46.158	NA	NA	F5	V338Vir	NA	1
	11.1059												

198.836	-	2.2	1.8108	8.8216	6.723	10.433	85.636	0.00	0.03	A8	UWVir	NA	1
	17.4714									IV/V			
201.669	-	1.0	2.5486	9.5171	6.2785	2.1003	85.011	0.005	0.025	A8V	BDVir	NA	1
	16.1046												
203.192	-17.759	0.14	0.4094	7.8799	3.4011	0.22645	277.84	0.025	0.03	F6V	LVVir	NA	1
205.697	-	0.2	0.4090	9.263	3.2808	0.050989	227.88	0.005	0.04	NA	BD -18	PPM	0
	18.8854										3667	717337	
211.968	-	0.7	2.3347	8.4074	6.3465	1.9933	38.449	NA	NA	F5	DMVir	NA	1
	11.1521												
211.626	-	0.3	0.7496	8.8799	5.0803	0.17877	79.244	0.015	0.11	A2III	FQVir	NA	1
	15.5078												
211.207	-	0.25	1.6936	8.7012	5.7877	0.14933	74.205	0.005	0.06	NA	BD -17	AKVir	1
	18.3606										3996		
212.364	-	0.35	0.7493	9.5831	4.2051	0.19179	121.97	0.025	0.06	F5V	CXVir	NA	1
	15.5816												
227.236	-	0.25	2.88475	7.2047	5.8387	0.95864	35.836	NA	NA	F2	ILLib	NA	1
	11.7905												
229.203	-	0.4	0.883	7.0607	3.9639	5.2944	119.92	0.005	0.04	A3IV	ESLib	NA	1
	13.0392												
232.32	-	0.2	1.27605	9.1309	5.2831	0.071499	103.16	0.005	0.14	A1IV	HD137914	NA	0
	14.4351												
232.966	-	0.35	0.3583	9.6686	3.2879	0.12395	169.29	0.015	0.05	F5	VZLib	NA	1
	15.6862												
234.948	-	0.2	0.797	9.726	3.6692	0.043077	184.94	0.015	0.08	A1/A2	HD139661	NA	0
	12.8062									III/IV			
234.306	-18.335	0.32	6.8617	7.9329	5.3866	0.94108	122.83	0.004	0.02	K1III	IVLib	BD -17	1
												4379B	
236.792	-	0.2	1.0944	9.5769	3.4825	0.083535	241.16	0.005	0.075	A2	HD141043	NA	0
	10.6215												
241.475	-	0.15	0.68175	9.5983	4.4546	0.032861	130.9	NA	NA	NA	BD -16	NA	0
	16.7817										4214		
241.605	-	0.2	0.9483	8.3735	3.7872	0.13228	170.33	0.05	0.035	A2V	HD144412	NA	0
	18.6567												
242.071	-	0.05	1.75875	7.9512	3.9072	0.0066278	135.87	0.025	0.08	A0V	V1283Sco	NA	1
	17.1348												
245.118	-12.911	0.06	2.7191	6.2926	6.4767	0.25589	161.32	0.01	0.02	F0	V1054Sco	NA	1
										III/IV			
252.365	-15.668	0.7	0.6614	6.0757	4.5305	117.58	256.26	0.005	0.03	A3V	V1010Oph	NA	1
252.731	-	0.15	2.1077	6.7612	5.6012	0.6219	208.46	0.00	0.025	B5V	V2355Oph	NA	1
	16.5469												
258.477	-	0.17	1.1951	8.0611	4.6524	0.20507	160.37	0.005	0.035	A9V	HD155684	NA	0
	18.2188												

263.582	-	0.15	2.6282	8.5106	3.57	0.14658	53.141	NA	NA	B9III	HD159246	NA	0
	18.5839												
266.238	-	0.05	2.35315	7.9179	3.921	0.21308	109.84	NA	NA	B9V	HD161225	NA	0
	13.5493												
266.903	-	0.025	12.451	5.8048	5.9658	1.5153	42.992	0.0	0.012	B9V	HD161701	NA	0
	14.7258												
269.851	-	0.85	2.1293	8.7559	5.646	1.1945	95.882	0.035	0.07	A2	WXSgr	NA	1
	17.3986									III/IV			
273.948	-	0.2	4.6717	8.0041	5.6725	0.07271	34.117	0.01	0.03	B5III	HD167398	HD167412	0
	18.4224												
272.64	-	0.06	7.8075	6.8742	5.1733	0.2302	50.363	0.393	0.02	B1II	HD166286	BD -16	0
	16.7493											4736P	
273.655	-	0.3	0.6996	9.8555	4.0551	0.5291	132.89	NA	NA	NA	BD -13	NA	0
	13.4002										4889		
275.454	-	0.035	1.3827	6.4552	4.1802	0.1946	109.19	0.005	0.08	B9V	HD168702	V4390Sgr	1
	16.3246												
274.259	-	0.3	3.4535	8.8313	4.3047	0.19809	115.05	0.025	0.04	B2/B3	VSer	NA	1
	15.5087									III			
277.105	-	0.3	3.4085	7.9229	5.3509	0.37642	107.49	0.00	0.025	B1/B2	V2349Sgr	NA	1
	16.7012									Ib			
276.160	-	0.16	10.2706	8.0667	4.091	0.32749	124.63	0.025	0.04	B3n	WSct	NA	1
	13.6748												
282.204	-	0.03	4.7907	5.4828	3.9456	0.072968	44.876	0.500	0.02	A2V	HIP 92307	CCDM	0
	18.6322											J18488	
282.714	-	0.2	1.57295	8.9156	3.3882	0.17838	93.953	NA	NA	A9	HD174397	-1838AB	0
	13.9092											NA	
283.613	-	0.3	0.95835	8.9229	4.6523	0.279	162.2	0.005	0.08	A9	USct	NA	1
	12.6098												
286.491	-	0.45	0.7148	7.9042	3.3453	3.9489	215.73	0.005	0.025	B2/B3	V4197Sgr	NA	1
	19.4813									V			
288.756	-	0.08	0.875	7.7244	4.64	0.28778	132.32	0.015	0.06	B9	HD179923	BD -16	0
	15.9766									IV/V		5215B	
294.679	-	0.23	3.7186	8.3576	5.9003	0.12296	38.655	0.01	0.04	B8V	HD185229	NA	0
	17.0942												
295.571	-	0.125	3.7067	8.3026	5.8637	0.043614	54.159	0.002	0.02	A0V	HD185990	NA	1
	14.9705												
298.277	-	0.8	1.1829	6.4019	5.2705	94.422	155.64	0.005	0.015	A1V	V505Sgr	NA	1
	14.6032												
297.611	-	0.08	6.074	7.2224	6.2693	0.066809	45.529	NA	NA	B6III	HD187439	NA	0
	13.9239												

304.484	-	0.25	3.3921	8.8321	5.6064	0.2062	56.448	NA	NA	A1	RWCap	NA	1
	17.6731									III/IV			
302.504	-	0.09	5.5376	7.7802	5.7766	7.3784	53.202	0.03	0.02	F5V	HD191365	HD191430	0
	13.0464												
303.839	-	0.2	0.6364	9.4584	4.5911	12.766	222.62	0.025	0.08	A9V	HD192450	NA	0
	12.6246												
306.124	-	0.45	1.4235	9.5064	5.8738	50.299	117.51	0.01	0.035	A5III	TYCap	NA	1
	12.9654												
305.214	-	0.4	0.69955	9.9763	5.1104	3.0141	125.17	0.015	0.07	A5	UWCap	NA	1
	10.5152												
306.785	-	0.13	1.0798	7.6587	3.7731	0.46354	327.51	0.01	0.035	F0	BHCap	NA	1
	11.5473												
308.604	-	0.18	7.346	9.2075	5.3282	0.0081122	137.82	0.00	0.05	K1III	BD -11	NA	0
	10.6828										5364		
307.511	-	0.05	1.9980	8.3212	5.9416	2.8639	59.2	NA	NA	F8	HD195181	NA	0
	10.0758												
310.453	-	0.25	0.5124	8.7696	4.7275	4.0739	157.1	NA	NA	F3V	HD197090	NA	0
	13.9043												
313.949	-	0.08	1.0748	6.8846	3.375	0.13401	219.73	0.025	0.06	F7V	HD199143	AZCap	1
	17.1142												
312.829	-	0.07	0.807	7.3746	3.52	0.20018	196.77	0.015	0.05	F0V	NPAqr	NA	1
	13.9244												
312.430	-	0.2	0.5861	8.5199	3.6104	0.45042	203.34	0.015	0.04	A5	SV*	OOAqr	1
	13.1265									IV/V	BV1717		
311.534	-	0.4	2.52715	9.2787	7.08	0.66414	49.435	NA	NA	G0	HD197777	NA	0
	11.3438												
314.707	-	0.26	1.5755	5.807	4.8596	8.4242	158.54	0.015	0.06	K0	HD358087	DVAqr	1
	14.5001												
314.648	-	0.5	5.7826	7.0746	7.2661	1.6567	24.215	0.0	0.014	G2/G3	HD199587	NA	1
	13.3685									V			
314.901	-	0.05	2.2413	6.2104	3.5554	0.24023	116.97	0.065	0.14	Ap	AOCap	NA	0
	19.0353												
318.577	-	0.1	0.4191	8.8622	3.06	0.065375	187.91	0.025	0.08	F6IV	HD202131	HD202203	0
	13.8896												
320.28	-	0.05	0.5627	8.2740	3.5015	0.030002	161.54	0.025	0.06	F3V	HD203190	HD203161	0
	11.6867												
320.067	-	0.9	1.9666	8.4764	7.4309	3.1889	57.605	0.01	0.03	A3	RYAqr	NA	1
	10.8023												
320.872	-	0.33	0.6617	10.504	3.1758	0.34573	185.49	0.005	0.20	F5	HD358446	NA	0
	11.1275												
321.636	-	0.35	0.6908	8.5995	3.7531	0.35279	205.59	0.015	0.04	A9V	CQCap	NA	1
	17.8785												

324.954	-	0.21	2.959	8.8822	3.9324	0.41874	188.31	0.015	0.05	K0	ADCap	NA	1
	16.0058									IV/V			
323.237	-17.564	0.3	6.7156	8.3946	4.9643	0.49337	133.77	0.005	0.03	K0III	HD205032	NA	0
322.049	-	0.15	0.4773	9.6387	3.4737	0.020116	151.55	0.025	0.15	F8	HD204300	BD -19	0
	19.1004											6102B	
326.76	-	0.15	1.0228	2.8337	5.4122	107.4	128.8	0.005	0.04	A6m	delCap	NA	1
	16.1266												
330.609	-	0.28	0.9450	6.0641	5.6883	5.5757	133.9	0.005	0.045	NA	CCDM	DXAqr	1
	16.9648										J22024		
334.908	-	0.2	0.8846	9.503	3.8571	0.03637	172.39	0.005	0.1	F0V	HD211750	NA	0
	14.3124												
337.687	-	0.42	0.4076	9.7315	4.0316	0.17653	218.58	0.025	0.08	F6/F7V	HD213321	NA	0
	13.5436												
336.434	-18.693	0.1	0.7357	9.154	4.0186	0.038585	279.07	0.025	0.06	NA	BD -19	HD212561	0
											6272		
338.118	-	0.27	0.6389	10.399	4.0963	0.032927	242.77	0.025	0.07	A2	HD213537	NA	0
	18.9711												
340.478	-12.4	0.15	3.3953	9.0714	6.6144	0.011307	47.59	NA	NA	G0V	HD214934	NA	0
340.034	-	0.055	1.88275	8.2237	6.7596	0.0072071	49.433	NA	NA	F3V	CCDM	NA	0
	15.9588										J22401		
343.016	-	0.5	1.0447	9.4601	5.5955	0.42465	114.3	0.025	0.12	A2IV	SUAqr	NA	1
	12.9455												
340.142	-	0.25	1.0273	10.569	4.3901	0.048501	124.39	0.015	0.08	K2V	2MASS	NA	1
	15.7891										J22403402		
348.863	-	0.1	3.3025	8.8777	4.1945	0.01125	112.8	0.025	0.08	A3II	HD219387	NA	0
	12.3715												
351.449	-	0.15	1.5943	9.3253	4.3647	0.062115	112.25	0.015	0.08	A2III	HD220687	NA	1
	11.6099												
352.508	-	0.3	0.4455	8.8916	3.4634	2.3354	285.5	0.015	0.06	F8V	BD-12-	HD221165	1
	11.9084										6502		
239.419	-	0.43	9.1999	5.7287	5.5398	12.261	28.862	0.0	0.006	B3V	NSV 7359	NA	0
	20.9831												
253.886	-	0.02	3.7399	6.3529	3.7192	0.0059572	85.297	NA	NA	B9III	CCDM	NA	0
	21.5695										J16555		
254.344	-	0.2	8.793	8.2323	3.5348	0.10286	66.112	0.0	0.02	A1IV	-2134AB	NA	1
	25.7996										UUOph		
261.295	-	0.09	1.6942	7.8548	3.8281	0.058072	57.763	NA	NA	B9	CD -24	NA	0
	24.6052										13328		

264.92	-	0.33	3.12695	8.7633	3.9533	0.25973	67.086	NA	NA	A2	V846Oph	NA	1
	28.8534												
265.099	-	0.045	0.9215	6.7874	4.5101	0.14926	141.9	0.035	0.10	B3Vne	HD160319	NA	0
	28.9232												
266.772	-	0.5	2.5197	8.5183	4.8781	1.7697	120.32	0.035	0.06	F3V	BNSgr	NA	1
	28.1499												
267.116	-	0.14	2.6187	6.034	4.6453	1.7625	190.21	0.005	0.05	B4IVe	HIP87163	NA	1
	26.9749												
270.245	-	0.3	4.6712	8.3064	3.4461	0.42562	96.239	0.035	0.08	B4III	WYSgr	NA	1
	23.0322												
270.702	-	0.12	1.5194	7.2747	5.2504	0.43214	138.64	NA	NA	B3II	V5562Sgr	NA	1
	29.3766												
270.865	-	0.35	1.3193	7.6687	5.0436	1.1983	154.22	0.0	0.06	B3nn	V4202Sgr	NA	1
	22.6462												
272.255	-	0.42	2.248	6.4448	3.7614	9.05	176.97	0.005	0.06	B9IV	CSI -25 - 18059	V3792Sgr	1
	25.4921												
272.363	-	0.15	1.7442	6.9113	4.3734	0.71551	157.86	0.005	0.07	B6III	HIP88943	NA	0
	24.0186												
275.577	-	1.5	3.2755	8.537	6.8388	1.6201	38.873	NA	NA	A2/A3 IV	XZSgr	NA	1
	25.2639												
281.968	-	0.5	4.44825	6.7588	7.8399	34.33	97.941	NA	NA	B9III	V356Sgr	NA	1
	20.2745												
285.728	-	0.25	1.1619	9.0931	4.7485	0.37938	115.62	NA	NA	A4 II/III	V523Sgr	NA	1
	29.1427												
287.737	-25.911	0.28	11.7899	8.2783	3.5682	0.26594	28.664	0.134	0.007	B9V	V5570Sgr	NA	1
289.464	-	0.1	4.8142	8.4851	3.7519	0.30322	75.183	0.002	0.02	A6IV	HD180520	NA	0
	24.7061												
290.228	-	0.075	1.6669	8.1335	3.97	6.1353	84.66	0.025	0.1	F0V	HD181292	NA	0
	23.8356												
291.126	-	0.035	0.5214	5.8645	4.098	0.24242	275.79	0.065	0.08	B2Vn	HR7355	HD182120	0
	27.8659												
293.013	-	0.28	1.4398	7.4899	4.7352	2.4628	194.82	0.005	0.03	B8V	V5572Sgr	NA	1
	28.2124												
294.734	-	0.035	3.4753	6.6342	3.7624	0.15006	291.57	0.025	0.06	B9	V4062Sgr	NA	0
	28.6072												
295.664	-	0.125	0.7224	7.465	3.9348	2.616	198.95	0.005	0.1	NA	TYC 6894 48 1	V4063Sgr	0
	24.4329												
297.735	-	0.13	1.1715	8.4906	4.7148	0.211	163.02	0.005	0.05	A5III	CCDM J19509 -2638AB	NA	0
	26.6387												
297.803	-	0.18	3.5036	9.4256	3.3937	1.011	34.81	NA	NA	F5V	HD187533	NA	1
	20.5028												

300.15	-	0.015	1.6652	6.3824	4.8303	0.063667	69.175	NA	NA	K0III	HD189365	V1173Sgr	1
	28.5864												
304.496	-	0.13	1.177	8.001	4.1505	0.45996	239.69	0.015	0.035	G2III	V4374Sgr	NA	1
	28.1331												
312.091	-	0.055	5.15195	6.9182	5.5004	0.017026	24.025	NA	NA	F7V	NLTT 49905	NA	0
	22.7407												
310.147	-	0.013	1.3399	7.4484	3.9504	0.077899	75.090	0.025	0.14	A4III	HD196816	NA	0
	27.5866												
315.743	-	0.15	0.7226	9.5378	4.6812	0.074199	188.17	0.035	0.15	G8V	HD200244	NA	0
	22.9336												
321.889	-	0.15	0.48225	9.9485	4.3722	0.041294	163.15	0.025	0.12	G8V	TYC 6372 1266 1	NA	1
	20.9133												
321.236	-	0.18	0.7156	9.5101	3.7546	0.11808	219.69	0.025	0.08	F4V	HD203798	NA	0
	21.6525												
324.401	-	0.25	1.4741	7.7244	6.7401	1.0809	155.22	0.005	0.03	F3V	BQCap	NA	1
	20.4319												
324.153	-	0.27	0.5440	9.2615	4.1631	0.20773	287.69	0.02	0.055	F5V	HD205563	NA	0
	22.2997												
328.575	-	0.13	2.4465	9.3474	7.3198	0.053594	74.716	0.004	0.03	Fm	HD208090	NA	0
	22.9645												
258.437	-	0.4	5.7282	7.5473	3.9281	2.9865	120.46	0.005	0.04	B6V	FVSCO	NA	1
	32.8526												
259.714	-31.583	0.19	1.6201	8.6409	4.8226	0.4785	152.00	0.005	0.05	B3	V474SCO	NA	1
262.304	-	0.075	2.5136	6.6946	5.2055	0.39186	149.19	0.065	0.04	O9.5V	V1081SCO	NA	1
	31.5343												
262.805	-	0.3	1.17345	8.8562	5.3651	0.66093	144.63	0.005	0.06	B5	V700SCO	NA	1
	31.3785												
262.26	-	0.38	1.1667	7.6921	4.541	3.2044	164.56	0.005	0.03	B1III	V499SCO	NA	1
	33.0045												
281.522	-30.489	0.6	4.15415	8.7902	4.9901	1.4934	98.102	NA	NA	A9V	SXSgr	NA	1
283.174	-	0.16	1.4517	6.4872	4.4953	2.1661	186.67	0.01	0.03	B8V	V4407Sgr	NA	1
	30.7341												
283.886	-	0.11	2.8124	8.4159	6.3134	0.14475	76.435	NA	NA	B9V	HD175162	NA	0
	32.0235												
286.806	-	0.3	0.7051	7.5461	4.3497	3.0389	234.00	0.005	0.065	A6V	V525Sgr	NA	1
	30.1605												
287.063	-	0.3	1.9193	9.2647	4.9514	0.30954	95.852	0.13	0.04	A0V	V526Sgr	NA	1
	31.3486												

REFERENCES

- Auvergne, M. et al. 2009, *Astronomy and Astrophysics*, pp 411–424
- Bewsher D., Brown D. S., Eyles C. J., Kellett B. J., White G. J., Swinyard B., 2010, *Solar Physics*, pp 1–28
- Brown D. S., Bewsher D., Eyles C. J., 2009, *Solar Physics*, 254, 185
- Claret A., Willems B., 2002, *Astronomy and Astrophysics*, 388, 518
- de Mink S. E., Langer N., Izzard R. G., 2010, Arxiv preprint arXiv:1010.2200
- Eyles C. J., Harrison R. A., Davis C. J., Waltham N. R., Shaughnessy B. M., Mapson-Menard H. C. A., Bewsher D., Crothers S. R., Davies J. A., Simnett G. M., et al., 2009, *Solar Physics*, 254, 387
- Hussain G., Allende Prieto C., Saar S., Still M., 2006, *Monthly Notices of the Royal Astronomical Society*, 367, 1699
- Kaiser M. L., Kucera T. A., Davila J. M., St. Cyr O. C., Guhathakurta M., Christian E., 2008, *Space Science Reviews*, 136, 5
- Kamiński K., Ruciński S., Matthews J., Kuschnig R., Rowe J., Guenther D., Moffat A., Sasselov D., Walker G., Weiss W., 2007, *The Astronomical Journal*, 134, 1206
- Koch D. G., Borucki W. J., Basri G., Batalha N. M., Brown T. M., Caldwell D., Christensen-Dalsgaard J., Cochran W. D., DeVore E., Dunham E. W., et al., 2010, *The Astrophysical Journal Letters*, 713, L79
- Kovács G., Zucker S., Mazeh T., 2002, *Astronomy and Astrophysics*, pp 369–377
- Kozai Y., 1962, *The Astronomical Journal*, 67, 591
- Mathieu R. D., Mazeh T., 1988, *The Astrophysical Journal*, 326, 256
- O’Brien M., Bond H., Sion E., 2001, *The Astrophysical Journal*, 563, 971
- Oksala M. E., Wade G. A., Marcolino W. L. F., Grunhut J., Bohlender D. A., Manset N., Townsend R. H. D., the MiMeS Collaboration 2010, ArXiv e-prints
- Pollacco D. L., Skillen I., Cameron A. C., Christian D. J., Hellier C., Irwin J., Lister T. A., Street R. A., West R. G., Anderson D., et al., 2006, *Publications of the Astronomical Society of the Pacific*, 118, 1407
- Prsa A., Batalha N. M., Slawson R. W., Doyle L. R., Welsh W. F., Orosz J. A., Seager S., Rucker M., Mjaseth K., Engle S. G., Conroy K., Jenkins J. M., Caldwell D. A., Koch D. G., Borucki W. J., 2010, ArXiv e-prints
- R Development Core Team 2008, *R: A Language and Environment for Statistical Computing*. R Foundation for Statistical Computing, Vienna, Austria
- Scargle J. D., 1982, *Astrophysical Journal*, 263, 835
- Southworth J., Maxted P. F. L., Smalley B., 2005, *Astronomy and Astrophysics*, 429, 645
- Stassun K. G., Mathieu R. D., Valenti J. A., 2006, *Nature*, 440, 311
- Torres G., Lacy C. H., Marschall L. A., Sheets H. A., Mader J. A., 2006, *The Astrophysical Journal*, 640, 1018
- VandenBerg D. A., Bergbusch P. A., Dowler P. D., 2006, *The Astrophysical Journal Supplement Series*, 162, 375
- Vanmunster T., 2008, *Peranso Light Curve and Period Analysis Software*. CBA Belgium Observatory
- Welch D. L., Stetson P. B., 1993, *AJ*, 105, 1813
- Zacharias N., Monet D., Levine S., Urban S., Gaume R., Wycoff G., 2004, *Bulletin of the American Astronomical Society*, 36, 1418